The Astrophysical Journal Supplement Series, 241:38 (35pp), 2019 April https://doi.org/10.3847/1538-4365/ab10df

A Comprehensive Analysis of *Spitzer* Supernovae

Tamás Szalai[1,2], Szanna Zsíros[1], Ori D. Fox[3], Ondřej Pejcha[4,8], and Tomás Müller[5,6,7,9]

[1] Department of Optics and Quantum Electronics, University of Szeged, H-6720 Szeged, Dóm tér 9., Hungary; szaszi@titan.physx.u-szeged.hu
[2] Konkoly Observatory, MTA CSFK, Konkoly-Thege M. út 15-17, Budapest, 1121, Hungary
[3] Space Telescope Science Institute, 3700 San Martin Drive, Baltimore, MD 21218, USA
[4] Institute of Theoretical Physics, Faculty of Mathematics and Physics, Charles University in Prague, Czech Republic
[5] Millennium Institute of Astrophysics, Santiago, Chile
[6] Instituto de Astrofísica, Pontificia Universidad Católica de Chile, Av. Vicuña Mackenna 4860, 782-0436 Macul, Santiago, Chile
[7] Department of Physics and Astronomy, University of Southampton, Southampton, Hampshire, SO17 1BJ, UK
Received 2018 March 5; revised 2019 February 25; accepted 2019 March 15; published 2019 April 23

Abstract

The mid-infrared (mid-IR) wavelength regime offers several advantages for following the late-time evolution of supernovae (SNe). First, the peaks of the SN spectral energy distributions shift toward longer wavelengths, following the photospheric phase. Second, mid-IR observations suffer less from effects of interstellar extinction. Third, and perhaps most important, the mid-IR traces dust formation and circumstellar interaction at late times (>100 days) after the radioactive ejecta component fades. The *Spitzer Space Telescope* has provided substantial mid-IR observations of SNe since its launch in 2003. More than 200 SNe have been targeted, but there are even more SNe that have been observed serendipitously. Here we present the results of a comprehensive study based on archival *Spitzer*/IRAC images of more than 1100 SN positions; from this sample, 119 SNe of various subclasses have been detected, including 45 SNe with previously unpublished mid-IR photometry. The photometry reveals significant amounts of warm dust in some cases. We perform an in-depth analysis to constrain the origin and heating mechanism of the dust, and present the resulting statistics.

Key words: circumstellar matter – infrared: stars – supernovae: general

Supporting material: machine-readable tables

1. Introduction

Tracing the multiwavelength evolution of supernovae (SNe) over many years, and even decades, can provide important clues about the shock physics, circumstellar environment, and dust production. The current ground-based transient surveys ensure the optical follow-up of hundreds of SNe per year, but these observations are typically at early times, during the photospheric phase. Late-time optical spectra and/or non-optical observations are rarer because they require large apertures or space telescopes.

The *Spitzer Space Telescope* (hereafter *Spitzer*) has been the primary source of mid-infrared (mid-IR) observations of many SNe. Between 2003 and 2009, in the cryogenic (or Cold Mission) phase, only a moderate number (<50) of nearby SNe were targeted by *Spitzer*. Since 2009, even with post-cryogenic (Warm Mission) *Spitzer*, over 150 more SNe have been targeted. Two surveys, in particular, contributed to this surge: a program aimed to observe a large sample of SNe IIn (73 observed SN sites, 13 detected targets; see Fox et al. 2011, 2013) and the SPitzer InfraRed Intensive Transients Survey (SPIRITS), a systematic mid-IR study of nearby galaxies (Kasliwal et al. 2017). SPIRITS has resulted in the detection of 44 objects of various types of SNe (observing 141 sites; Tinyanont et al. 2016), three obscured SNe missed by previous optical surveys (Jencson et al. 2017, 2018), and a large number of other variables and transients, including ones with unusual infrared behavior (Kasliwal et al. 2017).

These mid-IR observations have several advantages over optical observations, including increased sensitivity to the ejecta as it expands and cools, less impact by interstellar extinction, and coverage of atomic and molecular emission lines generated by shocked gas as it cools (see, e.g., Reach et al. 2006). Most of the mid-IR observations are sensitive to warm dust in the SN environment. The origin and heating mechanism of the dust, however, are not always obvious as the dust may be newly formed or pre-existing in the circumstellar medium (CSM). Newly condensed dust may form in either the ejecta or in a cool dense shell (CDS) produced by the interaction of the ejecta forward shock with a dense shell of CSM (see, e.g., Pozzo et al. 2004; Mattila et al. 2008; Smith et al. 2009). Pre-existing dust may be radiatively heated by the peak SN luminosity or by X-rays generated by late-time CSM interaction, thereby forming an IR echo (see, e.g., Bode & Evans 1980; Dwek 1983; Graham & Meikle 1986; Sugerman 2003; Kotak et al. 2009). In this case, the dust is a useful probe of the CSM characteristics and the pre-SN mass loss from either the progenitor or companion star (see, e.g., Gall et al. 2011 for a review).

Based on theoretical expectations (see, e.g., Kozasa et al. 2009; Gall et al. 2011), Type II-P explosions are likely the best candidates for dust formation among SNe. Some of these objects were targets of *Spitzer* observations in the early years of the mission. These data typically trace dust formation ~1–3 yr after explosion and estimate the physical parameters of newly formed dust. In addition to several detailed studies of single objects (e.g., Meikle et al. 2006, 2007, 2011; Sugerman et al. 2006; Kotak et al. 2009; Andrews et al. 2010; Fabbri et al. 2011; Szalai et al. 2011), Szalai & Vinkó (2013) presented an

[8] Lyman Spitzer Jr. Fellow.
[9] LSSTC Data Science Fellow.

analysis of 12 SNe II-P, yielding nine detections and three upper limits. The results do not support the theoretical prediction of significant ($\gg 0.001\,M_\odot$) dust production in SNe or the large dust masses observed in some old SN remnants and/or high-redshift galaxies. Several ways to reconcile this inconsistency include imperfections of grain condensation models, the probability of clumping dust formation, or significant grain growth in the interstellar matter (see Gall et al. 2011, as well as Szalai & Vinkó 2013, for a review). Another possibility is that a significant amount of dust may be present in the form of very cold (<50 K) grains in the ejecta, but to date, far-IR and submillimeter observations have only been able to detect such dust in the very nearby case of SN 1987A (Matsuura et al. 2011, 2015; Indebetouw et al. 2014; Wesson et al. 2015).

SNe IIn exhibit signatures of interaction between the ejecta and dense CSM. This shock interaction may lead to either heating of pre-existing circumstellar grains or dust condensation in the CDS that can form between the forward and reverse shocks. Papers on individual objects (e.g., Gerardy et al. 2002; Fox et al. 2010; Andrews et al. 2011a; Gall et al. 2014), together with the comprehensive *Spitzer* study of SNe IIn mentioned above (Fox et al. 2011, 2013), show how the mid-IR evolution can be used to the trace the mass-loss history of the progenitor in the years leading up to the SN.

In contrast with the relatively large number of Type II-P and IIn SNe with published *Spitzer* data, there are fewer published mid-IR observations of thermonuclear explosions of C/O white dwarfs (SNe Ia) or stripped-envelope core-collapse SNe (SE CCSNe; including Type Ib/c, Ibn, and IIb ones). Historically, these SN subclasses are less likely to form new dust, due to their high ejecta velocities, and less likely to have pre-existing, dense CSMs. For example, Chomiuk et al. (2016) and Maeda et al. (2015b) used radio and near-IR observations, respectively, to place strict upper limits on the amount of material surrounding SNe Ia.

In recent years, however, many SNe within the SNe Ia and stripped-envelope subclasses have shown signs of a dense CSM and/or warm dust. One example is SNe Ia-CSM, which are thought to be thermonuclear explosions exploding in dense, H-rich shells of ambient CSM (producing IIn-like emission features in their late-time spectra; see, e.g., Silverman et al. 2013; Fox et al. 2015; Inserra et al. 2016) and are very bright in mid-IR, even 3–4 yr after explosion (Fox & Filippenko 2013; Graham et al. 2017). The subluminous thermonuclear Type Iax SN 2014dt showed an excess of mid-IR emission (over the expected fluxes of more normal SNe Ia) at ~1 yr after explosion (Fox et al. 2016; see also in Section 3.2), and an excess of near-IR emission was observed by circumstellar dust around the super-Chandrasekhar candidate SN 2012dn (Yamanaka et al. 2016; Nagao et al. 2017).

Some stripped-envelope SNe show mid-IR emission at late times, too. For example, the Type Ic SN 2014C showed an excess of mid-IR emission develop ~1 yr post-explosion (Tinyanont et al. 2016), as did several SNe IIb, including SN 2013df (Szalai et al. 2016; Tinyanont et al. 2016) and SN 2011dh (Helou et al. 2013). The SN Ibn subclass, which shows narrow helium lines, do not typically show a late-time mid-IR excess (with respect to the expected flux level originating from the cooling ejecta). However, the Type Ibn SN 2006jc was bright in early-time *Spitzer* images (Mattila et al. 2008).

Despite the relatively high number of SNe with reported *Spitzer* observations, most of the analysis consists of single-object papers. There have been some broader studies on SNe IIn (Fox et al. 2011, 2013), SNe II-P (Szalai & Vinkó 2013), and SNe Ia (Johansson et al. 2017), and a SPIRITS summary by Tinyanont et al. (2016), which includes observations of ~140 CCSNe within 20 Mpc.

The motivation of the current work, however, is to provide a complete review of all SNe currently in the *Spitzer* archive to compare the mid-IR properties of different SN subclasses. This paper includes mid-IR observations of more than 1100 SN positions, from which 119 objects have been detected. Within this detected sample, many observations were previously unpublished and 45 targets were observed serendipitously during other science programs.

In Section 2, we describe the steps of the data collection and photometry of *Spitzer*/IRAC (Infrared Array Camera) data. We present our results in Section 3, including a statistical analysis of the mid-IR evolution of the different SN subclasses and simple model fits to the spectral energy distributions (SEDs). Finally, the conclusions of our study are presented in Section 4.

2. Observations and Data Analysis

2.1. Collection of Supernova Data from the Spitzer *Heritage Archive*

Using the list of SNe on the website of the Central Bureau for Astronomical Telegrams[10] and the website of the All-Sky Automated Survey for Supernovae (ASAS-SN; Shappee et al. 2014; Holoien et al. 2017a, 2017b, 2017c),[11] we selected all SNe that were discovered before 2015 and have been spectroscopically classified. We also selected additional nearby ($z \lesssim 0.05$) SNe listed in the Open Supernova Catalog[12] (Guillochon et al. 2017). This search returned ~4500 objects, all of which have had their positions searched in the *Spitzer* Heritage Archive[13] (SHA; using a 100″ environment for the queries). We found 1142 SN sites that have been observed post-explosion with *Spitzer*. For these SNe, we downloaded the available IRAC data for further analysis, whether or not the data had been previously published. We note that although Multiband Imaging Photometer and Infrared Spectrograph data can also contribute to the understanding of the mid-IR behavior of SNe (see, e.g., Kotak et al. 2006, 2009; Gerardy et al. 2007; Fabbri et al. 2011; Szalai et al. 2011; Szalai & Vinkó 2013), only a few objects observed with these instruments exist so we focus only on IRAC data in this article.

2.2. Object Identification and Photometry on Spitzer*/IRAC Images*

We collected and analyzed all available IRAC post-basic calibrated data (PBCD). The scale of these images is 0″.6/pixel. Identifying a point source at the position of an SN explosion can be difficult at the large distances to some of these galaxies, where compact H II regions or the host clusters of SNe may also appear as point-like sources on *Spitzer*/IRAC images. Furthermore, the target can be faint or on top of a complex background.

[10] http://www.cbat.eps.harvard.edu/lists/Supernovae.html

[11] http://www.astronomy.ohio-state.edu/~assassin

[12] https://sne.space

[13] http://sha.ipac.caltech.edu

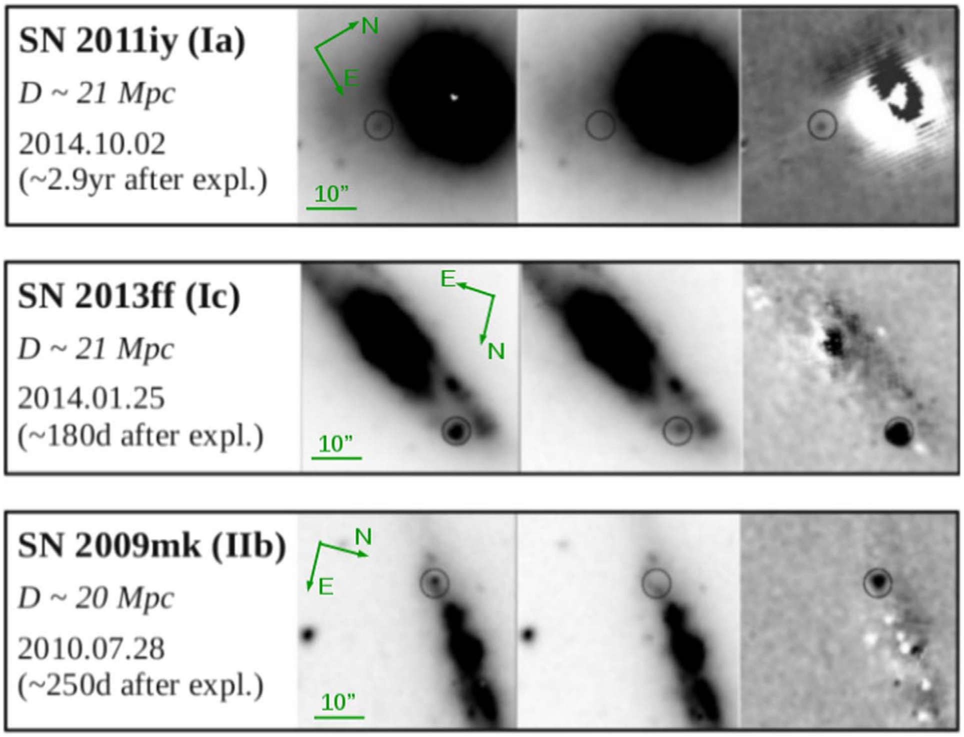

Figure 1. HOTPANTS template subtraction of our *Spitzer* data. For each SN, the three panels show the (left) most recent *Spitzer*/IRAC 4.5 μm image, (center) template, and (right) differenced image.

We therefore performed image subtraction with HOTPANTS[14] whenever a template exists (Figure 1). This procedure achieved a good match between the background levels of target and template frames, resulting in net background levels close to zero in the subtracted images. However, not all targets have templates. In these cases, the local background was estimated by measuring actual flux fluctuations by placing apertures covering the region of the SN site. In all cases (including either image-subtracted or non-subtracted images), we defined the source as a positive detection if (i) the source showed epoch-to-epoch flux changes, and (ii) its flux was above the local background by at least 5 μJy and 15 μJy at 3.6 and 4.5 μm, respectively (according to point-source sensitivities in Table 2.10 of the IRAC Instrument Handbook version 2).

Moreover, in some cases, only a single-epoch set of *Spitzer* observations is available, thus, epoch-to-epoch flux changes cannot be used as indicators of the presence of SNe. In these cases, as a first step, we used archival pre-explosion 2MASS JHK_s images in order to exclude the potential false-positive detections (compact H II regions, etc.). For precise astrometric comparison, we collected the absolute coordinates of the SNe concerned from the Open Supernova Catalog and derived their (x, y) coordinates in the *Spitzer*/IRAC images (note that the uncertainties of the absolute SN coordinates have not been reported in the most cases). *Spitzer*/IRAC post-BCD images have a pointing to 2MASS with an accuracy of $0\farcs15$ (see IRAC Instrument Handbook[15]); an additional limit is the $0\farcs6$/pixel resolution of *Spitzer*/IRAC PBCD images. The basic astrometric criterion of a potential positive detection was an agreement between the absolute SN coordinates and the position of the photometric center of the mid-IR point source within two IRAC pixels ($1\farcs2$). In the second step, we carried out aperture photometry on the pre-explosion 2MASS *JHKs* images (using the same aperture and annulus/dannulus parameters as those during the *Spitzer* photometry). Because, in most cases, there are no detectable point sources on the 2MASS images at the positions of the SNe, it was not possible to estimate reliable photometric errors based on photon statistics; instead, we have used a ± 0.4 mag value as a general photometric error, based on the upper limit of 2MASS photometric uncertainties reported in Skrutskie et al. (2006). In order to reveal the presence of any possibly real mid-IR excess at post-explosion *Spitzer*/IRAC images, we have fitted simple blackbodies (BBs) to the SEDs consisting of the upper limits of pre-explosion 2MASS photometry (assuming a general uncertainty of 0.4 mag mentioned above). The photometric criterion of a positive detection was to find *Spitzer*/IRAC fluxes being above the fitted SED with a 3σ photometric error in at least one IRAC channel. Conclusively, we labeled in total seven SNe with single-epoch *Spitzer* data as positive detections; we note that all of these SNe are expected to show strong mid-IR radiation at the given epoch (strongly interacting SNe IIn or early-caught SNe of other types).

We performed a photometric analysis for all positive detections at every epoch. For isolated sources, we implemented aperture photometry on the PBCD frames using the `phot` task of IRAF[16] as a first step. We generally used an aperture radius of 2″ and a background annulus from 2″ to 6″ (2−2−6

[14] http://www.astro.washington.edu/users/becker/hotpants.html
[15] https://irsa.ipac.caltech.edu/data/SPITZER/docs/irac/iracinstrumenthandbook/

[16] IRAF is distributed by the National Optical Astronomy Observatories, which are operated by the Association of Universities for Research in Astronomy, Inc., under cooperative agreement with the National Science Foundation.

configuration), applied aperture corrections of 1.213, 1.234, 1.379, and 1.584 for the four IRAC channels (3.6, 4.5, 5.8, and 8.0 μm, respectively) as given in the IRAC Data Handbook, but sometimes used the 3−3−7 configuration (aperture corrections: 1.124, 1.127, 1.143, and 1.234, respectively) or the 5−12−20 configuration (aperture corrections: 1.049, 1.050, 1.058, and 1.068, respectively). For targets with templates, we compared the results before and after template subtraction to test for consistency. We generally found good agreement between the two methods ($\lesssim$10% difference in fluxes, which is within the approximated uncertainty of the *Spitzer*/IRAC photometry). In the few cases where the difference between the two methods was more than 10%, we preferred the results of image subtraction photometry.

For sources on top of complex backgrounds without a corresponding template, we implemented the photometric method described by Fox et al. (2011; called hereafter as the "Fox+11 method"). This method applies a set of single apertures with a fixed radius to estimate both the SN and average background flux. This technique allows us to visually identify only local background associated with the SN, as opposed to the annuli of the aperture configurations mentioned above.

We compared our results to any previously published *Spitzer*/IRAC SN photometry. In general, we found good agreements with the published values ($\lesssim$10% difference in fluxes). In a few cases, the flux differences are larger, but each of these cases consists of either a very faint target and/or complex sky background.

The target details and resulting mid-IR photometry of all SNe with previously unpublished *Spitzer* photometry are listed in Tables 4 and 5, respectively. We clearly highlight SNe identified on a single-epoch set of *Spitzer* images, as well as all the other SNe where image subtraction cannot be applied; in all these cases, measured fluxes are strictly handled as upper limits. Flux uncertainties in Table 5 are generally based on photon statistics provided by `phot`, but, where photometry was carried out on subtracted images, the increment of the noise level by $\sqrt{2}$ is also taken into account. We present all pairs of images (*Spitzer*/IRAC + pre-explosion 2MASS K_s) and SED fittings we used to select the single-epoch positive detections, together with an example for negative detections, in Appendix B.

3. Results

3.1. Demographics

The total number of observed SN positions is over 1100. The majority of SNe are nearby ($z < 0.05$). We detect 119 SNe, including 45 objects that have no previously published *Spitzer* photometry. Only ∼12% of the SN sites were observed pre-explosion. We also highlight three specific targets (SNe 2012aw, 2012fh, and 2013ee), which have been noted by Tinyanont et al. (2016) as positive *Spitzer* detections, but without any corresponding photometry. We summarize the statistics of our SN sample in Table 1 and Figures 2 and 3.

About 40% of the objects (mostly Type Ia) are located in distant, anonymous galaxies, but these observations did not yield any SN detections. There are also ∼60 SNe that are also located in complex regions of the galaxy, typically very close to the galaxy nuclei. In these cases, even template subtraction is not effective, due to the asymmetric profile of the IRAC point-spread function (PSF). We do not include any of these SNe in this analysis.

Following the methods presented by Tinyanont et al. (2016), we present the detection rates separated in three time bins after discovery: less than one year, one to three years, and more than three years. If an SN is observed with at least one detection in a bin, it is considered detected, even though it might fade away later in the same bin.

3.2. Mid-IR Evolution: Trends and Outliers

Figure 4 plots the mid-IR photometry of all SNe with positive *Spitzer* detections. Table 6 lists all corresponding Vega magnitudes, distances, and $E(B-V)$ values. For plotting purposes, Figure 4 excludes some objects with decade-long mid-IR data sets—e.g., Type II-pec SN 1987A (Dwek et al. 2010) or Type II-L SN 1979C (Tinyanont et al. 2016)—but these SNe are included in our statistical analysis. Figures 5–9 highlight the SN subclasses so that individual SNe can be identified and photometric details can be ascertained. Tables 4 and 6 contain all sources of previously published *Spitzer* data we used for constructing Figures 2–9 and for the analysis we present below.

3.2.1. Thermonuclear SNe

This work more than doubles the number of SNe Ia with positive mid-IR detection (33 versus 15). Figure 5 shows that most SNe Ia have a relatively well-defined evolution compared to the other SN subclasses, consistent with previous results (Tinyanont et al. 2016; Johansson et al. 2017). The handful of Type Ia-CSM SNe, however, are extremely bright at mid-IR wavelengths. This sample is small, so it is difficult to draw any definitive conclusions about the overall trend. For example, PTF11kx ($D \sim 200$ Mpc) is still detectable at ∼1800 days, while SN 2002ic ($D \sim 280$ Mpc) faded at a similar age.

We do not find any previously unpublished SNe Ia with mid-IR fluxes comparable to those of known SNe Ia-CSM. This result suggests that a dense CSM is rare in the environments of thermonuclear SNe (which may also hint that SNe Ia-CSM arise from different progenitor systems than the majority of SNe Ia), or that CSM shells may be far away from the explosion sites. Based on the existing (rough) estimations, SN Ia-CSM objects may contribute between 1% and 5% of all SNe Ia (see, e.g., Meng & Podsiadlowski 2018), which seems to be supported by our results; however, future systematic surveys are necessary for the thorough study of this problem.

We do find some other SNe Ia that deviate from the expected mid-IR evolution. SNe 2010B and 2010gp, observed at early times, are noticeably brighter. Note, however, that SN 2010B has a complex background that may be contributing additional mid-IR flux. On the other hand, SN 2010gp has a template for subtraction, so these results are quite robust. SN 2011iy, which is relatively nearby ($d \sim 20$ Mpc), also appears as a point source at 4.5 μm after image subtraction ∼1030 days after explosion (see Figure 1). This SN, however, is not detectable at 3.6 μm.

SN 2014dt, classified as an SN Iax, should be also highlighted here: this object shows a clear and even growing mid-IR excess ∼1 yr after explosion, which has been explained with the presence of newly formed dust, pre-existing dust, or possibly a bound remnant (Foley et al. 2016; Fox et al. 2016). The only other SN Iax we identified as a mid-IR source on

Table 1
Statistics of the *Spitzer*/IRAC Data of the Sample of Studied SNe

	Thermonuclear SNe				SE CCSNe							SNe II				
	Ia	Ia-pec	Iax	Ia-CSM	Ib	Ib-pec	Ibn	Ib/c	Ic	Ic-pec	IIb	II-P	II-P pec.	IIn	II-L	Unclass. SN II
Total number of observed SN sites: 1142/693[a]																
Total number of observed SN sites	723/294[a]	25/23[a]	8	5	59/53[a]	1	2	1	73/63[a]	5/4[a]	25	36	2	101	4	72
SN sites with multiple observations: 553/334[a]																
SN sites with multiple observations	325/112[a]	9	4	5	27/25[a]	1	1	⋯	35/33[a]	3	14	32	2	38	4	53
SN sites with pre-explosion images: 111/87[a]																
SN sites with pre-explosion images	43/20[a]	3	2	⋯	10	⋯	1	⋯	9/8[a]	⋯	4	10	2	9	1	17
Total number of positive detections: 119																
Total number of positive detections	24	1	2	5	5	⋯	1	1	7	1	7	22	1	25	2	15
Unpublished positive detections: 45																
Unpublished positive detections	13	1	1	2	3	⋯	⋯	1	2	⋯	4	4	⋯	6	1	7

Note.
[a] Total number of objects/number of objects excluding SNe in distant, anonymous galaxies.

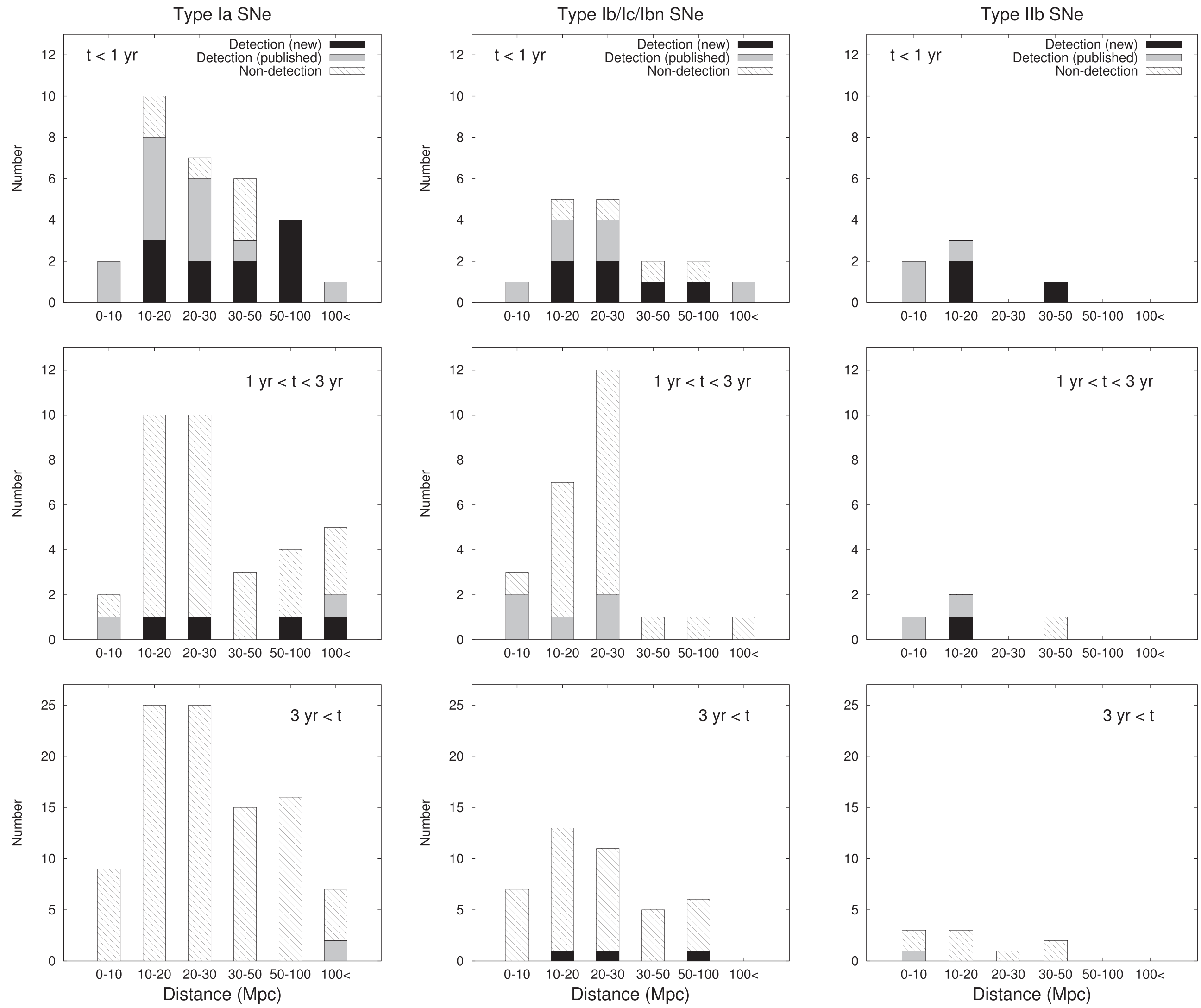

Figure 2. Statistics of detected Type Ia and stripped-envelope CCSNe in our *Spitzer*/IRAC sample. The statistics are divided by type and epoch. The number of detections is plotted as a function of distance in each case. We do not include SNe located in distant ($z \gtrsim 0.05$), anonymous galaxies and/or too close to the center of their hosts. We also exclude most SNe with only a single-epoch *Spitzer*/IRAC observations.

Spitzer images is SN 2005P. While SN 2005P seems to have a slight 8.0 μm detection at ∼180 days, there is no comparable data with SN 2014dt. By ∼1 yr post-explosion, SN 2005P has faded below the detection threshold.

3.2.2. Stripped-envelope CCSNe

Figure 6 plots the mid-IR absolute magnitudes of SE CCSNe. The stripped-envelope designation encompasses various subclasses, including SNe IIb, Ib, and Ic, so their mid-IR evolution exhibits a bit of heterogeneity, particularly at later times.

The mid-IR evolution of "normal" SNe Ib/Ic seem to be fastest among SE CCSNe. SN 2014C presents itself as a special case in which the explosion transforms from a "normal" Type Ib into a strongly interacting, Type IIn-like SN (Milisavljevic et al. 2015; Margutti et al. 2017). SN 2014C is located within NGC 7331, which has been followed extensively as part of the SPIRITS program. Tinyanont et al. (2016) showed a roughly constant IR luminosity in the first ∼800 days and a unique rebrightening at ∼250 days as the CSM interaction begins.

Another interesting object is SN 2001em, a strongly interacting Type Ib/c object, which generated strong X-ray, radio, and optical emission for ∼3 yr post-explosion (see Pooley & Lewin 2004; Soderberg et al. 2004; Stockdale et al. 2004; Chugai & Chevalier 2006). Unlike SN 2014C, however, the transformational process was not observed by *Spitzer*, making a direct comparison impossible. SN 2001em was observed by *Spitzer* only once. Figure 6 shows SN 2001em is even brighter than SN 2014C, although background contributions have not been removed. We present a more detailed analysis of SN 2001em in Section 3.3.

Finally, it is worth mentioning the one observation of SN 2011ft, a distant ($d \sim 100$ Mpc) SN Ib that is as bright as SN 2014C ∼250 days after explosion. With only a single 3.6 μm, more observations are planned.

Observations exist for only two SNe Ibn: SN 2006jc (four epochs, but only one from the first year) and PS1-12sk (one epoch). These two events are bright in mid-IR during the early-time CSM interaction, but the brightness declines quickly. Following the interpretation of Mattila et al. (2008), the early mid-IR radiation may arise from newly formed dust in the

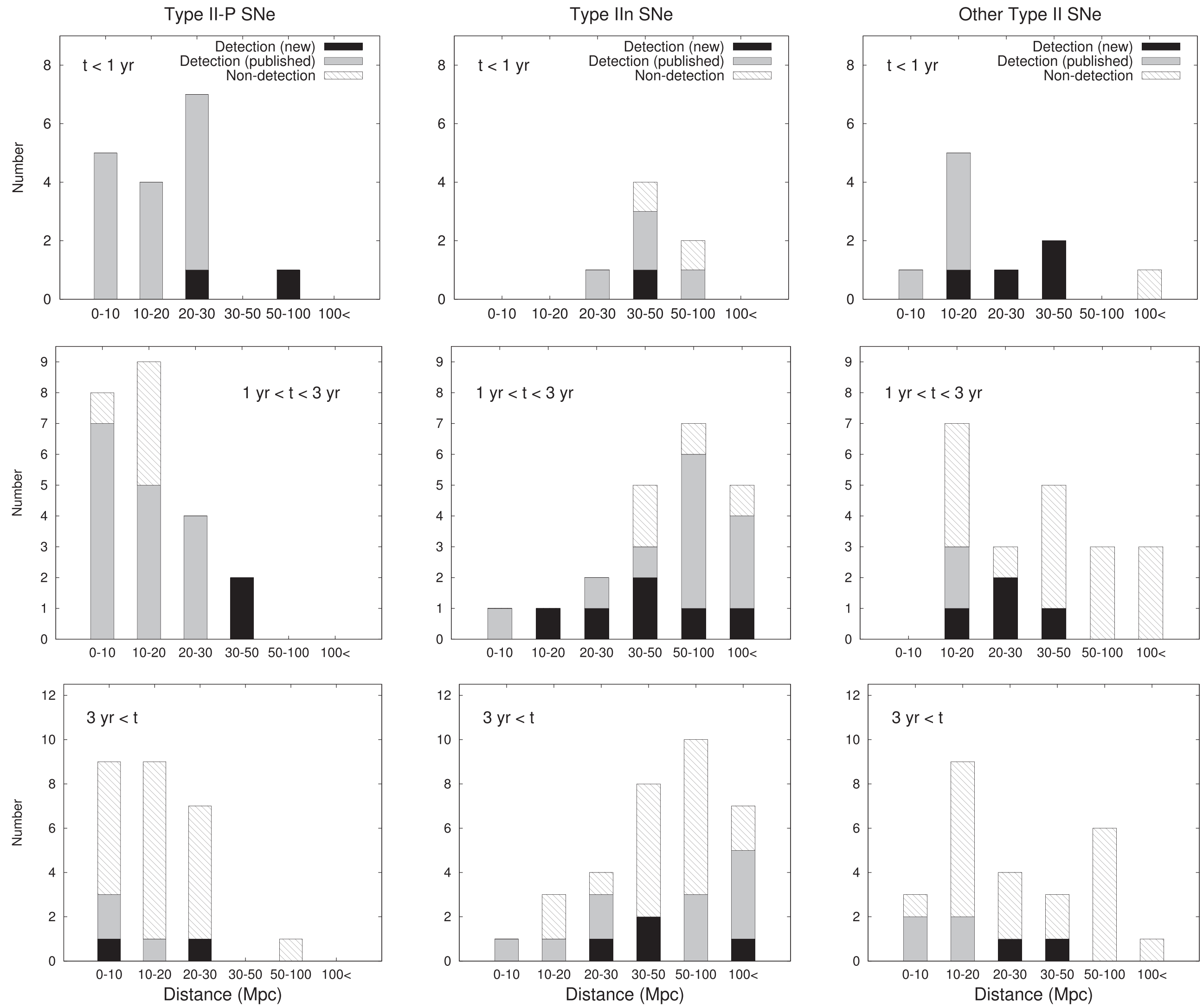

Figure 3. Same as Figure 2, except in this case for SNe II-P, Type IIn, and other (unclassified) SNe II.

CDS, while the source of the later-time mid-IR flux is probably an IR echo from pre-existing dust in the CSM.

Among SNe IIb, the moderately interacting SN 2013df (Maeda et al. 2015a; Kamble et al. 2016; Szalai et al. 2016) produces a slowly declining mid-IR light curve between ∼270–820 days (Szalai et al. 2016; Tinyanont et al. 2016). SN 2001gd shows a similar brightness at ∼950 days. SN 2011dh, one of the best-sampled SN in mid-IR, has also been detectable up to almost two years after explosion. The Type IIb SN 1993J ($D \sim 3.7$ Mpc) is detected >24 yr post-explosion in mid-IR (Tinyanont et al. 2016), while the Type IIb SN 2008ax ($D \sim 7.8$ Mpc) is not detected at even ∼4 yr after explosion.

The differences between SNe IIb seem to correlate with the assumed sizes of the progenitors of SE CCSNe. SNe 1993J, 2001gd, and 2013df, which are detected by *Spitzer* at later epochs, have been classified as Type eIIb objects (Chevalier & Soderberg 2010; Szalai et al. 2016), which denotes that these explosions originate from extended progenitors (yellow or red giants). SN 2008ax is known to be representative of Type cIIb objects, which are defined to have more compact progenitors, similar to those of SNe Ib/c. SN 2011dh seems to be an intermediate case in both its progenitor radius ($R\sim$ a few tens of $R_\odot$) and mid-IR evolution.

3.2.3. SNe II-P

Figure 7 plots the mid-IR absolute magnitudes of SNe II-P, which show a relatively homogeneous mid-IR evolution. Theoretical models suggest that the ejecta of most of SNe II-P may form dust between ∼300 and 600 days, due to the slow expansion velocities and high densities. Only a few SNe show evidence for a rebrightening in the mid-IR between ∼300 and 600 days: SNe 2004dj (Meikle et al. 2011; Szalai et al. 2011), 2011ja (Andrews et al. 2016; Tinyanont et al. 2016), and 2014bi (Tinyanont et al. 2016). This unexpectedly low rate may be influenced by the poor sampling of the other observed SNe II-P. Furthermore, while both SNe 2004dj and 2014bi show the rebrightening effect at 3.6 μm (with the first object showing rebrightening even at 5.8 and 8.0 μm; see Szalai et al. 2011), they are not detectable at 4.5 μm (there is a linear flux decline instead). Szalai et al. (2011) suggested that additional flux at 4.5 μm arises from the 1−0 vibrational band of CO at 4.65 μm (see Kotak et al. 2005) during the declining phase, but disappears

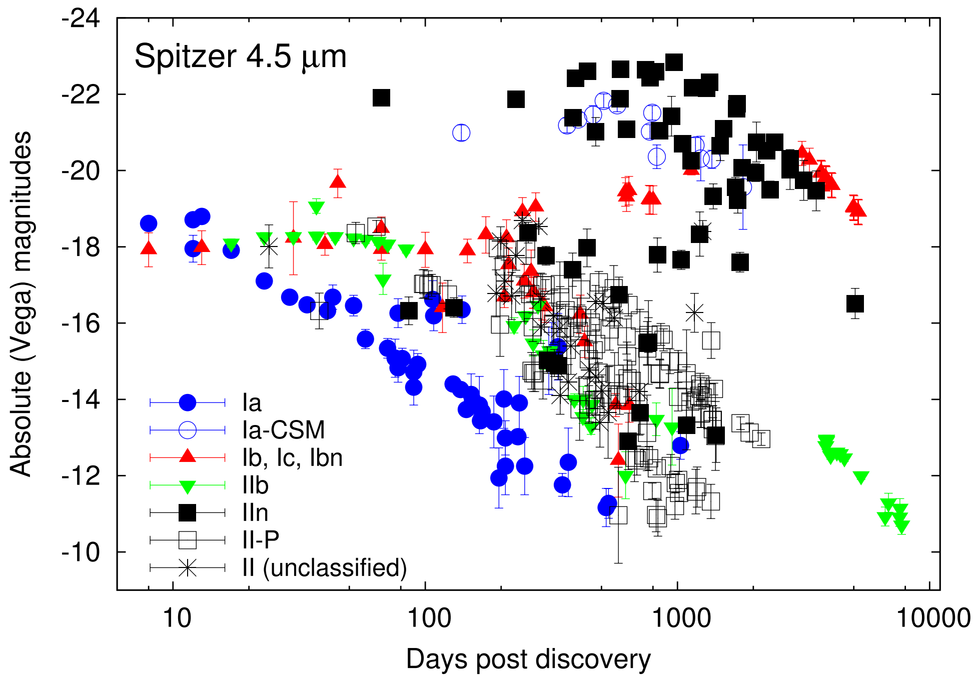

Figure 4. 4.5 μm absolute Vega magnitudes of all SNe identified as point sources in *Spitzer*/IRAC images. Values and sources of data are shown in Table 6.

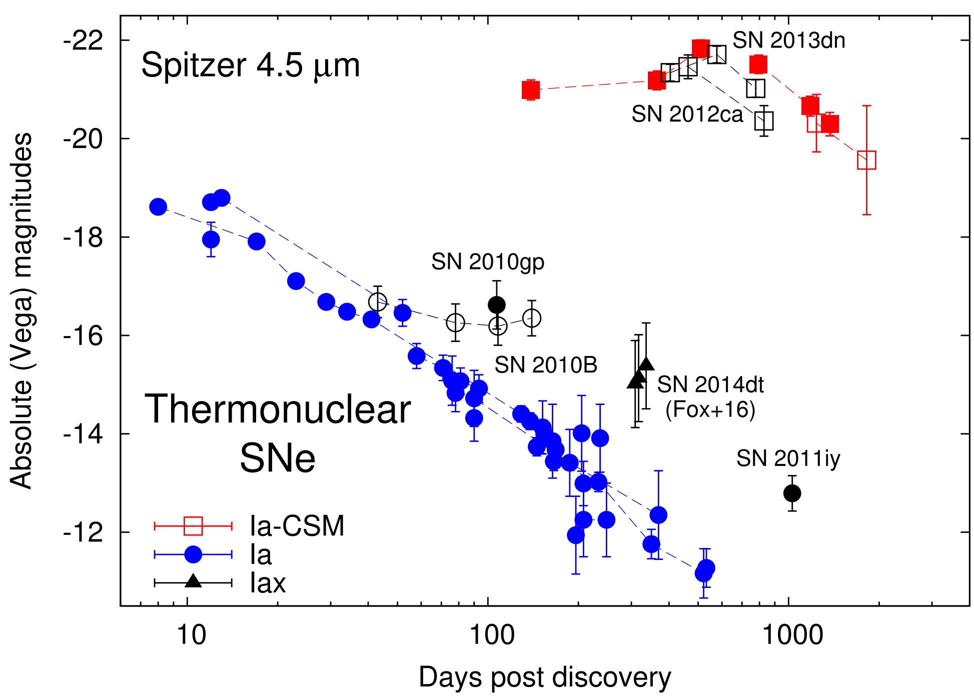

Figure 5. Mid-IR evolution of thermonuclear SNe; highlighted objects are marked with black symbols, while filled and empty symbols denote SNe whose absolute magnitudes were determined with or without template subtraction, respectively. Values and sources of data are shown in Table 6.

at ∼500 days (Szalai et al. 2011; Szalai & Vinkó 2013), thereby making 4.5 μm light curves difficult to interpret for SNe II-P.

Two other Type II-P SNe, 2004et (Kotak et al. 2009; Fabbri et al. 2011) and 2007oc (Szalai & Vinkó 2013) as well as the Type II-P/II-L SN 2013ej (Tinyanont et al. 2016; Mauerhan et al. 2017) also show mid-IR rebrightening, but it occurred between ∼700–1000 days. This rebrightening is detected at both 3.6 and 4.5 μm (at least in the cases of SNe 2004et and 2007oc; SN 2013ej becomes undetectable at 3.6 μm after ∼800 days). The above papers suggest this rebrightening is due to new dust forming in the CDS behind the reverse shock and not within the ejecta.

3.2.4. SNe IIn

Figure 8 plots the mid-IR absolute magnitudes of SNe IIn. For most SNe IIn, Fox et al. (2011, 2013) showed that the mid-IR radiation arises from pre-existing dust, which is radiatively heated by optical emission generated by ongoing interaction between the forward shock and CSM. Although many SNe IIn

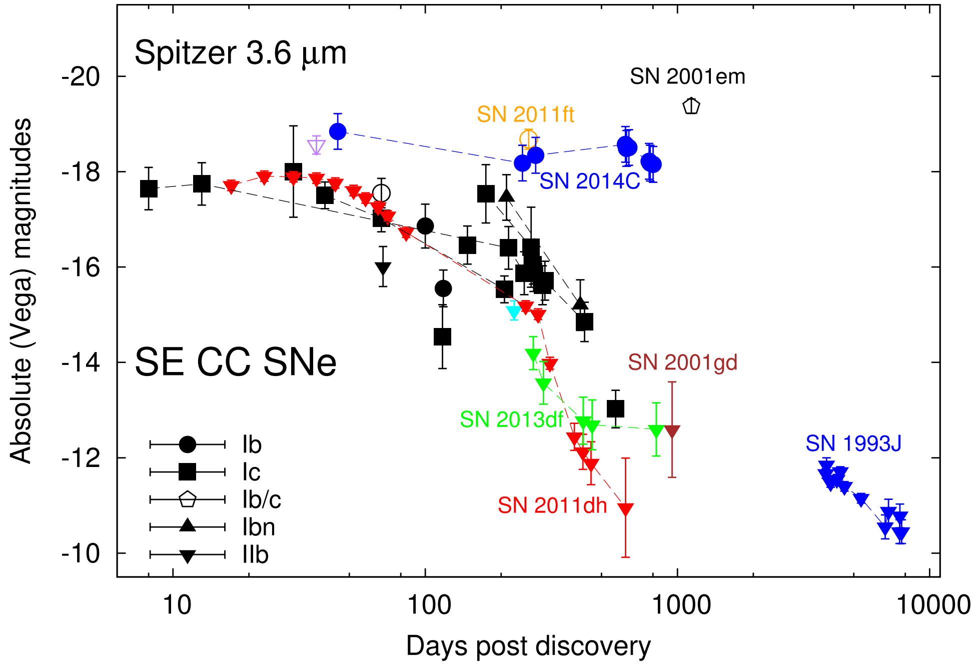

Figure 6. Mid-IR evolution of stripped-envelope core-collapse SNe; highlighted objects are marked with labels, while filled and empty symbols denote SNe whose absolute magnitudes were determined with or without image subtraction, respectively. Values and sources of data are shown in Table 6.

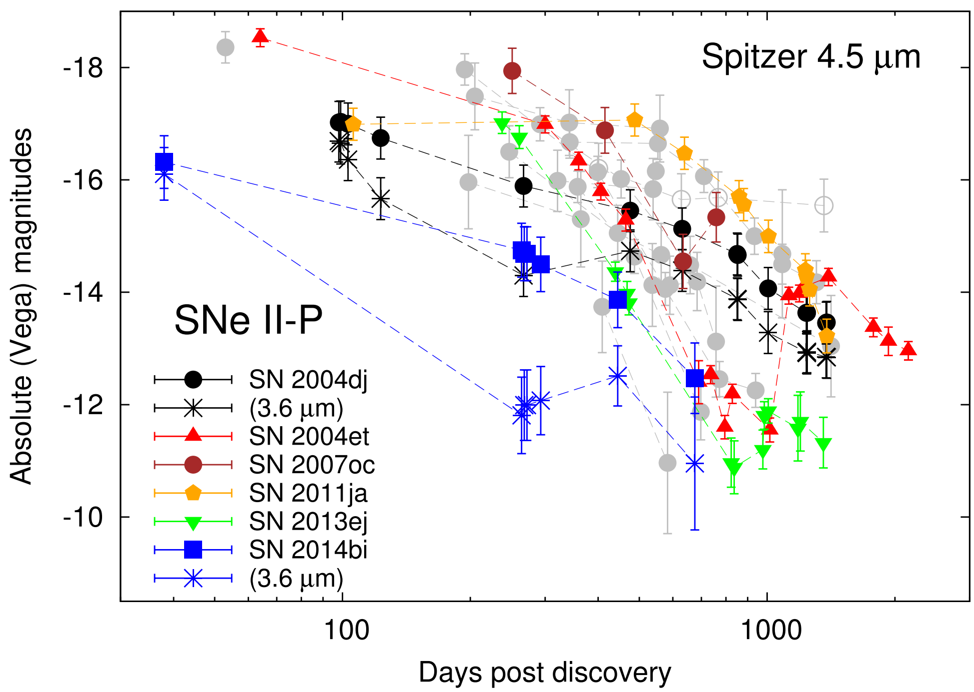

Figure 7. 4.5 μm absolute magnitudes of Type II-P explosions. Colored symbols denote objects where mid-IR rebrightening occurred. Filled and empty symbols denote SNe whose absolute magnitudes were determined with or without image subtraction, respectively. In two cases (SNe 2004dj and 2014bi), rebrightening can be only observed at 3.6 μm (see details in the text), the curves of which are also shown (marked with asterisks). All data are shown in Table 6.

show early evidence for CSM interaction (e.g., strong emission in Hα/X-ray/radio), only a handful of *Spitzer* observations exist in the first few months post-explosion. SNe 2009ip (Fraser et al. 2015, and this work) and 2011A were faint mid-IR sources in the first months, but both of these objects are considered low-luminosity Type IIn events/impostors (see the analyses of, e.g., Fraser et al. 2013, Mauerhan et al. 2013, Pastorello et al. 2013, Margutti et al. 2014, and de Jaeger et al. 2015). By contrast, SN 2010jl was extremely bright in mid-IR during the first year (Andrews et al. 2011a; Fox et al. 2013; Fransson et al. 2014; Williams & Fox 2015). The origin of the mid-IR excess has been debated, but it is likely a combination of both newly formed and pre-existing dust (Fransson et al. 2014; Gall et al. 2014).

The mid-IR evolution of SNe IIn is heterogeneous. While many SNe IIn remain bright for a year post-explosion, the decline rates are not always the same. Furthermore, many SNe

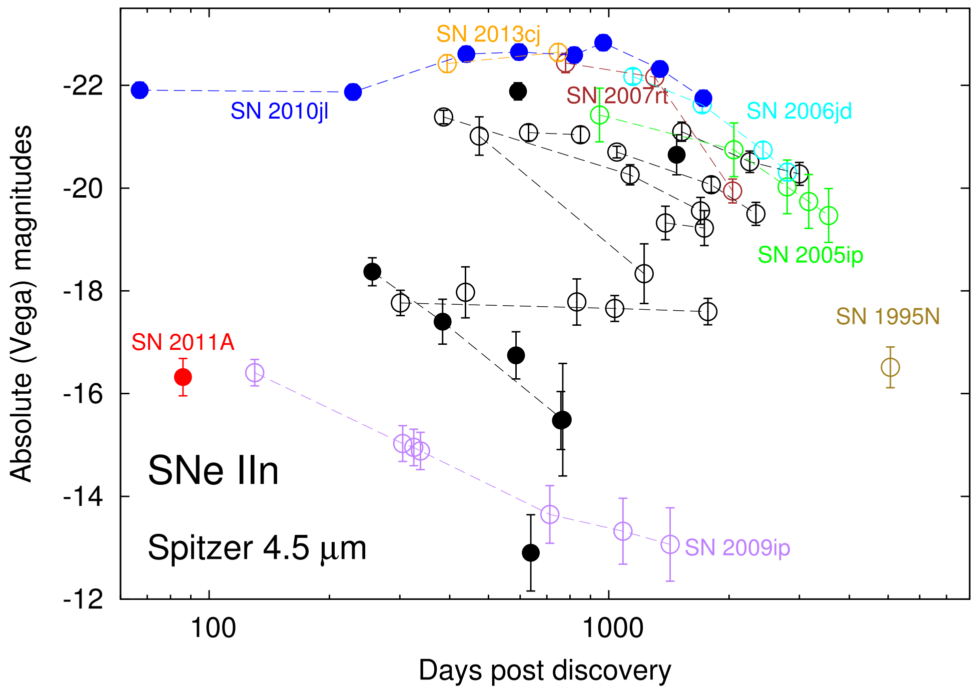

Figure 8. Mid-IR evolution of the Type IIn explosions studied. Highlighted objects are marked with colored symbols (see details in the text). Filled and empty symbols denote SNe whose absolute magnitudes were determined with or without image subtraction, respectively. In the case of SN 2009ip, epochs are defined relative to the large outburst that occurred in 2012. All of the data are shown in Table 6.

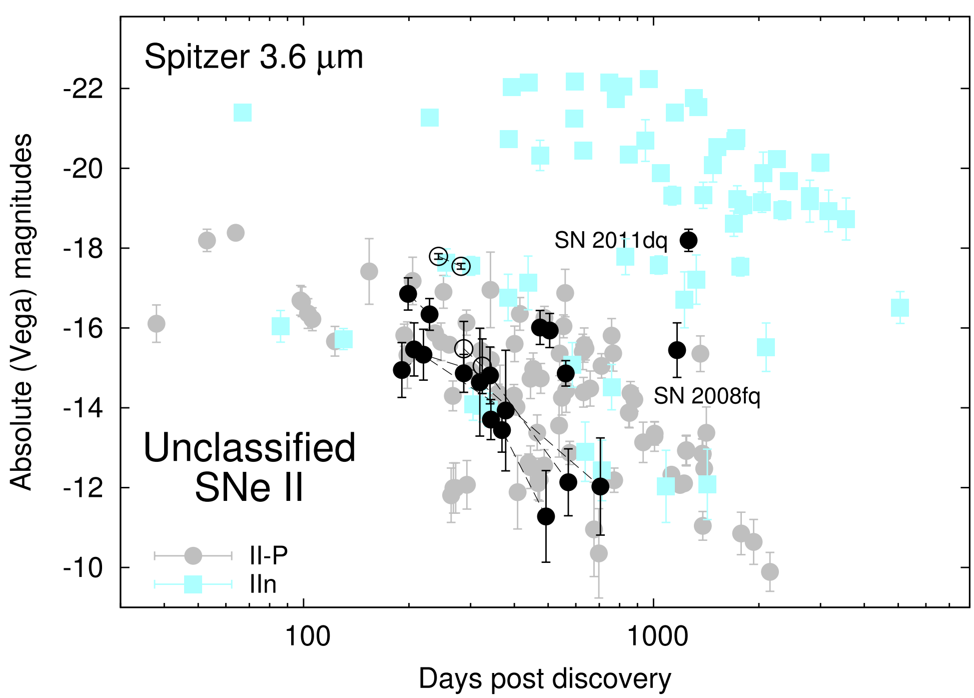

Figure 9. Mid-IR evolution of the unclassified SNe II in our sample (black symbols) compared to that of known SNe II-P and IIn (gray circles and rectangles, respectively). Filled and empty symbols denote SNe whose absolute magnitudes were determined with or without image subtraction, respectively (absolute magnitudes shown here are calculated from 3.6 μm fluxes, because several objects have been observed only at this wavelength). Values and sources of data are shown in Table 6.

IIn are not even detected (see Figure 3, as well as Fox et al. 2011). These differences likely correspond to the extent of pre-SN mass loss, but may also suggest different geometries, shock velocities, and progenitors.

Figure 4 shows that Type II-P and Type IIn SNe have quite distinct late-time mid-IR evolution. This dichotomy serves as a useful classification method for several unclassified targets in our sample (see Table 1). Most of these sources are likely Type

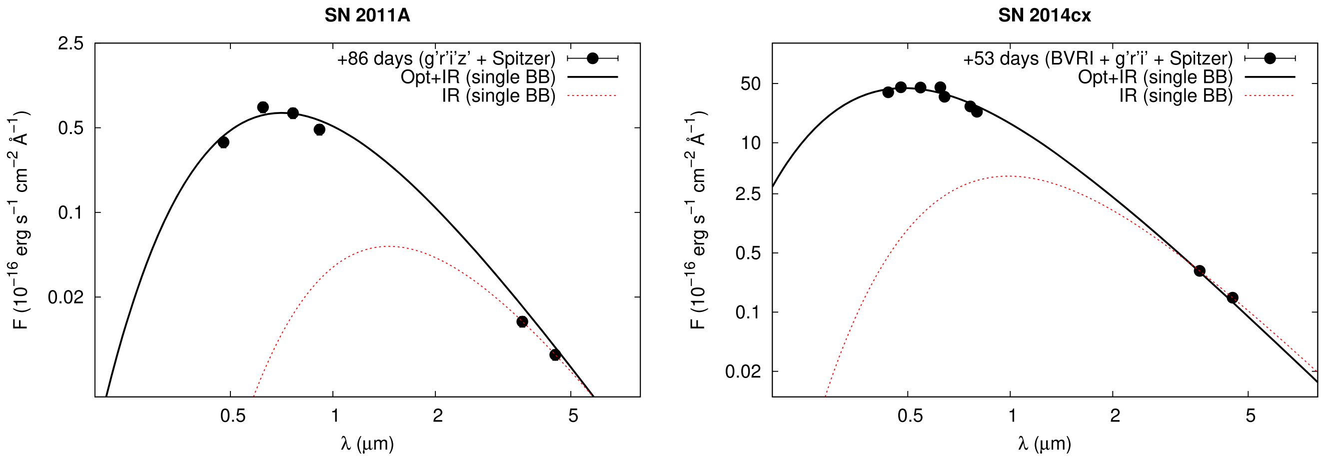

Figure 10. Comparison of single blackbody fits to the (left) Type IIn SN 2011A at +86 days, and (right) Type II-P SN 2014cx at +53 days. Fits are applied to both the combined optical−IR SEDs and only the mid-IR fluxes.

II-P, except SNe 2005kd, 2008fq, and 2011dq, which may be SNe IIn, as shown in Figure 9.

3.3. SED Fittings: Limitations, Methods, Consequences

Mid-IR SEDs of SNe span the peak of the thermal emission from warm dust and can place useful constraints on the dust properties (see, e.g., Kotak et al. 2009; Szalai et al. 2011; Szalai & Vinkó 2013). In most of our sample, these fits are limited to only two photometry points. Further challenges exist. During the first several months after explosion, a hot component arising from an optically thick gas in the innermost part of the ejecta may affect the continuum emission at these wavelengths. Moreover, the line emission by CO at 4.65 μm (described in Section 3.2.3) may also contribute a significant flux at 4.5 μm (although this effect has only been observed in some SNe II-P before ~500 days after explosion). Most of our sample with previously unpublished *Spitzer* data lack the multiwavelength data that can improve these fits. We also note that while the Galactic extinction (typically at a level below $E(B-V)=0.1$; see Table 4) is practically negligible at mid-IR wavelengths, the host 7galaxy extinction can be more important for both thermonuclear (see, e.g., Phillips et al. 2013) and CCSNe (see, e.g., Jencson et al. 2018, and references therein). Unfortunately, regarding most of the studied SNe, we have no information about the host extinction. As a simple estimation (based on the results of Xue et al. 2016), an extreme value of $E(B-V)_{\rm total}=1.0$ mag can attenuate the measured flux by ~20% at 3.6 or 4.5 μm.

We illustrate our fitting process using data from the SN IIn 2011A and SN II-P 2014cx. Both of these objects were observed by *Spitzer* within three months after explosion (at +86 and +53 days, respectively). In the case of SN 2011A, contemporaneous $g'r'i'z'$ data can be found in de Jaeger et al. (2015), and in the case of SN 2014cx, *BVRI* and $g'r'i'$ data obtained at the epoch of *Spitzer* observations can be found in Huang et al. (2016). The mid-IR fluxes were transformed to F_λ values and dereddened using the galactic reddening law parameterized by Fitzpatrick & Massa (2007) assuming $R_V=3.1$ and adopting the $E(B-V)$ values listed in Table 4.

Figure 10 shows that single-component BBs provide a good fit to the combined optical−IR SEDs of both SNe. Fitting only the mid-IR data yields significantly different parameters (see Table 2, which highlights the shortcomings of fitting just two data points). Regardless, the SED in this case does not show any evidence for an excess of mid-IR emission above the optically peaked SED.

The Type Ib SN 2009jf also has sufficient data to construct a combined optical−IR SED adopting *BVRI* measurements from Sahu et al. (2011b). *Spitzer* data were obtained at 100 days after explosion, while optical data are from +94 and +105 days. Unlike SNe 2011A and 2014cx, Figure 11 shows that SN 2009jf exhibits an excess at 4.5 μm, but not at 3.6 μm. Fitting the mid-IR data with a single BB is difficult.

Figure 12 shows data for the Type II-P SN 2012aw. The earliest *Spitzer* observations occur on day 358, and we extrapolate *V*-, *R*-, and *I*-band data from day ~330 (Dall'Ora et al. 2014). The hot component cannot be adequately modeled by a simple BB curve because the optical depth of the continuously expanding ejecta is quite low at this time. Therefore, we applied the global light-curve model of SNe II-P (Pejcha & Prieto 2015, hereafter called the PP15 model) to estimate the contribution of the hot component to the mid-IR fluxes. In order to construct the PP15 model SED, we calculated its values at the wavelengths of *BVRIJHK* filters, while, at longer wavelengths, we used the the Rayleigh−Jeans approximation ($F_\lambda \propto \lambda^{-4}$). Like SN 2009jf, there is an excess at 4.5 μm, indicating a warm dust component is present. Fitting this component is difficult with just two data points and is complicated even further by the potential 4.5 μm line emission in SNe II-P described above.

Finally, Figure 12 shows a similar analysis for the CSM-interacting Type II-P/II-L SN 2013ej (Leonard et al. 2013; Bose et al. 2015; Chakraborti et al. 2016; Dhungana et al. 2016; Kumar et al. 2016; Mauerhan et al. 2017). Despite the amount of published data, modeling of the combined (UV−)optical −IR SEDs has not been presented in the literature. Only one epoch (+236 days), however, has nearly contemporaneous mid-IR and optical data (Bose et al. 2015; Tinyanont et al. 2016, respectively). Like SN 2012aw, we fit the optical data with the PP15 model with parameters given by Müller et al. (2017). We ignore the *R*-band data in this case, however, given the strong Hα emission arising from CSM interaction (Bose et al. 2015; Huang et al. 2015; Dhungana et al. 2016; Mauerhan et al. 2017). The results for each fit are given in Table 3.

Table 2
Parameters of Single Blackbodies Fitted to the Optical-IR SEDs of SNe 2011A (IIn), 2014cx (II-P), 2009jf (Ib), and 2012aw (II-P)

	SN 2011A		SN 2014cx		SN 2009jf		SN 2012aw	
	(IIn, +86 days)		(II-P, +53 days)		(Ib, +100 days)		(II-P, +358 days)	
	R (10^{16} cm)	T (K)	R (10^{16} cm)	T (K)	R (10^{16} cm)	T (K)	R (10^{16} cm)	T (K)
Opt. + IR (single BB)	0.07	4100	0.13	5960	0.09	5760	0.05	3810
IR (single BB)	0.12	1990	0.23	2940	1.48	670	2.79	400

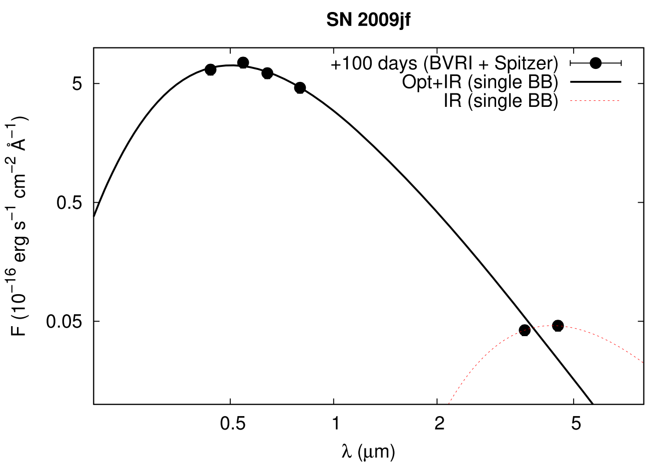

Figure 11. Comparison of single blackbody fits to the Type Ib SN 2009jf at +100 days. A fit is applied to both the combined optical−IR SEDs and only the mid-IR fluxes.

We performed a similar analysis of the rest of the targets in our sample. Because we are most interested in late-time emission and want to minimize contributions from the early-time photospheric light curve, we excluded targets that did not meet certain criteria. For example, we did not include SNe without late-time observations or only single-filter IRAC photometry. We also exclude "normal" SNe Ia because their mid-IR photometry do not probe warm dust (but see Nozawa et al. 2011).

For the SNe we analyze, we follow the method published in a number of papers (see, e.g., Meikle et al. 2007; Fox et al. 2010, 2011, 2016; Fox & Filippenko 2013; Szalai & Vinkó 2013; Graham et al. 2017) by assuming a spherically symmetric, optically thin dust shell. We calculate the minimum shell radius by fitting BBs ($R_{\rm BB}$) to the observed SEDs and, from the radii and the estimated ages, we also constrain the corresponding expansion velocities ($v_{\rm BB}$) by assuming a constant expansion over time (see Table 7).

For comparison, we also fit the analytic dust model adopted from Fox et al. (2010, 2011), assuming only thermal emission of optically thin dust with mass M_d, with a particle radius a, at a distance d from the observer, thermally emitting at a single equilibrium temperature T_d; hence, the flux can be written as

$$F_\nu = \frac{M_d B_\nu(T_d)\kappa_\nu(a)}{d^2}, \quad (1)$$

where $B_\nu(T_d)$ is the Planck function and κ_ν is the dust mass absorption coefficient as a function of the grain size. We chose pure graphite composition assuming single-size grains of $a = 0.1\ \mu$m (following Fox et al. 2010, 2011). During the fit, only T_d and M_d are free parameters; κ_ν has been determined from Figure 4 of Fox et al. (2010). In cases of two-point SEDs, we are limited to using one temperature component.

Figure 13 compares the analytical and BB fits in two SNe that have data from all four IRAC channels: the Type IIn SN 2002bu and the Type Ib/c 2001em. SN 2002bu was observed ∼2 yr post-explosion and can be fit with just a single-component graphite or BB dust model. SN 2001em, however, requires a two-component model. If we fit using BBs, we get the parameters shown in Figure 13. We can compare our results with those of Chugai & Chevalier (2006), who constructed a model for the strong late-time X-ray, radio, and Hα emission from SN 2001em and developed a picture in which the SN ejecta collide with a dense massive CS shell. Our two-component model gives $\sim 10^{16}$ cm and $\sim 15 \times 10^{16}$ cm for the two radii, which are compatible with the estimated size of the single CS shell ($r \sim 7 \times 10^{16}$ cm) calculated by Chugai & Chevalier (2006) from X-ray, radio, and Hα data contemporaneous with mid-IR observations. If we change the longer wavelength BB to a graphite dust model, we get $T_{\rm dust} = 280$ K and an upper limit of $M_{\rm dust} \approx 0.2\,M_\odot$, which are in a good agreement with the calculations of Chugai & Chevalier (2006), who derived—indirectly—300 K for dust temperature and 2–3 $M_\odot$ for the mass of the CS shell (which gives dust mass of 0.02–0.03 $M_\odot$ assuming a 0.01 dust-to-gas mass ratio). These results strengthen previous conclusions of CSM interaction with SN 2001em, but further suggest the presence of multiple pre-explosion dust shells.

Table 7 lists and Figures 14–17 plot the best-fit dust parameters (masses, temperatures, mid-IR luminosities). We fitted SEDs of all listed SNe using the dust model described above in order to generate a comparable set of dust parameters. Nevertheless, in general, one cannot distinguish between dust compositions with only two IRAC filters. We include the results of silicate fits only in cases with spectroscopic evidence, such as SN 2004et (Kotak et al. 2009; Fabbri et al. 2011) or SN 2005af (Szalai & Vinkó 2013). In some other cases, the temperature may provide guidance on the dust composition. For example, if $T_{\rm dust} \gtrsim 1400$ K, then the carbonaceous dust model makes the most sense because Si grains require lower temperatures for effective condensation (see, e.g., Nozawa et al. 2003).

Different dust models (composition, grain size) used in the literature result in systematic uncertainties in dust parameters. After comparing our results with previously published ones, we draw the following conclusions: the uncertainties can be as large as ∼100–150 K in dust temperature (which is also significantly influenced by the number of SED points including additional optical and/or near-IR data), while dust masses and dust luminosities can vary within one order of magnitude and within a factor of ∼1–2, respectively. We also note that choosing nonspherical geometry for the dust-forming region or assuming clumpy dust formation (see, e.g., Ercolano et al. 2007;

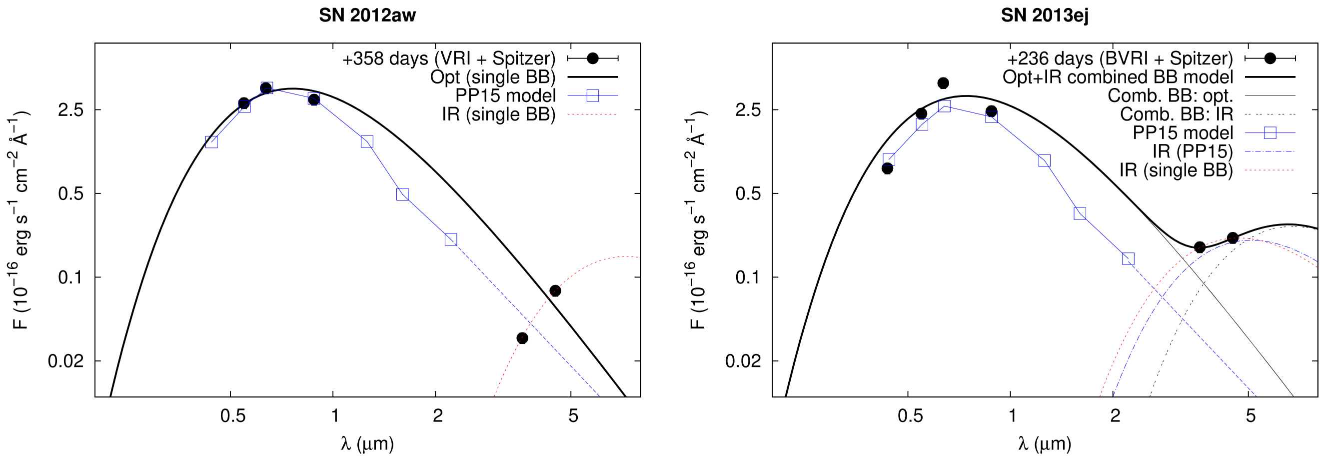

Figure 12. Comparison of single blackbody fits to the (left) SN 2012aw at +358 days and (right) SN 2013ej at +236 days. Fits are applied to both the combined optical−IR SEDs and only the mid-IR fluxes. SEDs calculated using the PP15 model are marked with open rectangles.

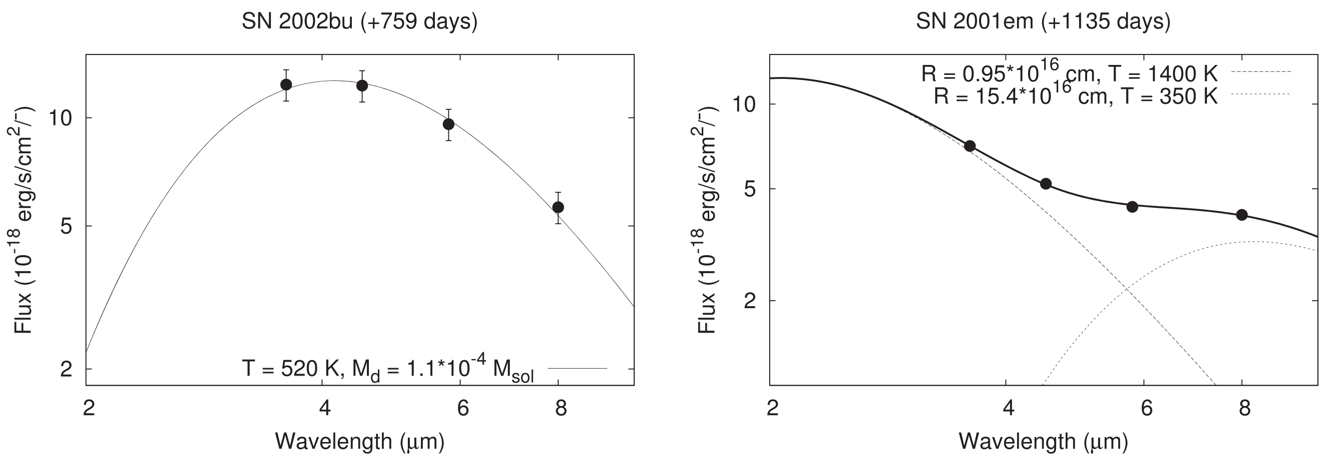

Figure 13. Left: one-component carbonaceous dust model fit to the four-point mid-IR SED of the Type IIn SN 2002bu. Right: two-component blackbody model fit to the four-point mid-IR SED of the known interacting Type Ib/c SN 2001em.

Table 3
Parameters of Two- and One-component Blackbodies Fitted to the Combined Optical−IR SED of the Known Interacting Type II-P/II-L SN 2013ej, Together with Dust Parameters Determined from Fitting a Simply Analytic Dust Model Comparing with Previously Published Results of Tinyanont et al. (2016)

	SN 2013ej (II-P/II-L, +236 days)						
	R_{opt} (10^{16} cm)	T_{opt} (K)	R_{IR} (10^{16} cm)	T_{IR} (K)	T_{dust} (K)	M_{dust} ($10^{-5}\,M_{\odot}$)	L_{dust} ($10^{6}\,L_{\odot}$)
Two-comp. BBs	0.05	3910	3.48	430	360	580	5.3
Opt. (PP15) + IR BB	⋯	⋯	1.51	570	460	98.8	3.3
IR (single BB)	⋯	⋯	1.25	620	490	69.9	2.9
Tinyanont et al. (2016) − IR	⋯	⋯	⋯	⋯	477	75.0	2.7

Meikle et al. 2007; Andrews et al. 2016) may also lead to significantly (an order of magnitude lower/higher) different calculated dust masses.

While the SED fits in Table 7 have a number of uncertainties, we can still draw some useful conclusions. The BB expansion velocities (v_{BB}), shown in the bottom-right panels of Figures 14–17, can distinguish between newly formed and pre-existing dust. In cases where v_{BB} is quite low (several hundreds or a few thousands km s^{-1}), the dust likely formed in the ejecta. In these cases, covering many Type II-P and SE CCSNe, we find the estimated temperatures and dust masses ($\sim10^{-6}$–$10^{-2}\,M_{\odot}$) are in agreement with this scenario (see, e.g., Fox et al. 2011, 2013; Szalai & Vinkó 2013; Tinyanont et al. 2016).

In cases where v_{BB} is a bit higher ($\sim$5000–15,000 km s^{-1}), the velocities are consistent with the forward shock, suggesting new dust may be forming in the CDS behind the forward shock. Nevertheless, especially in the cases of SNe IIn or Ia-CSM, or other known interacting objects (e.g., SN Ib 2014C) with large ($>10^{-3}\,M_{\odot}$) observed dust masses, the presence of pre-existing dust should be invoked to explain the amount of observed mid-IR luminosities. For the distinction between the collisional and radiative heating scenarios, we adopt the method presented in Fox et al. (2011; and also used by, e.g.,

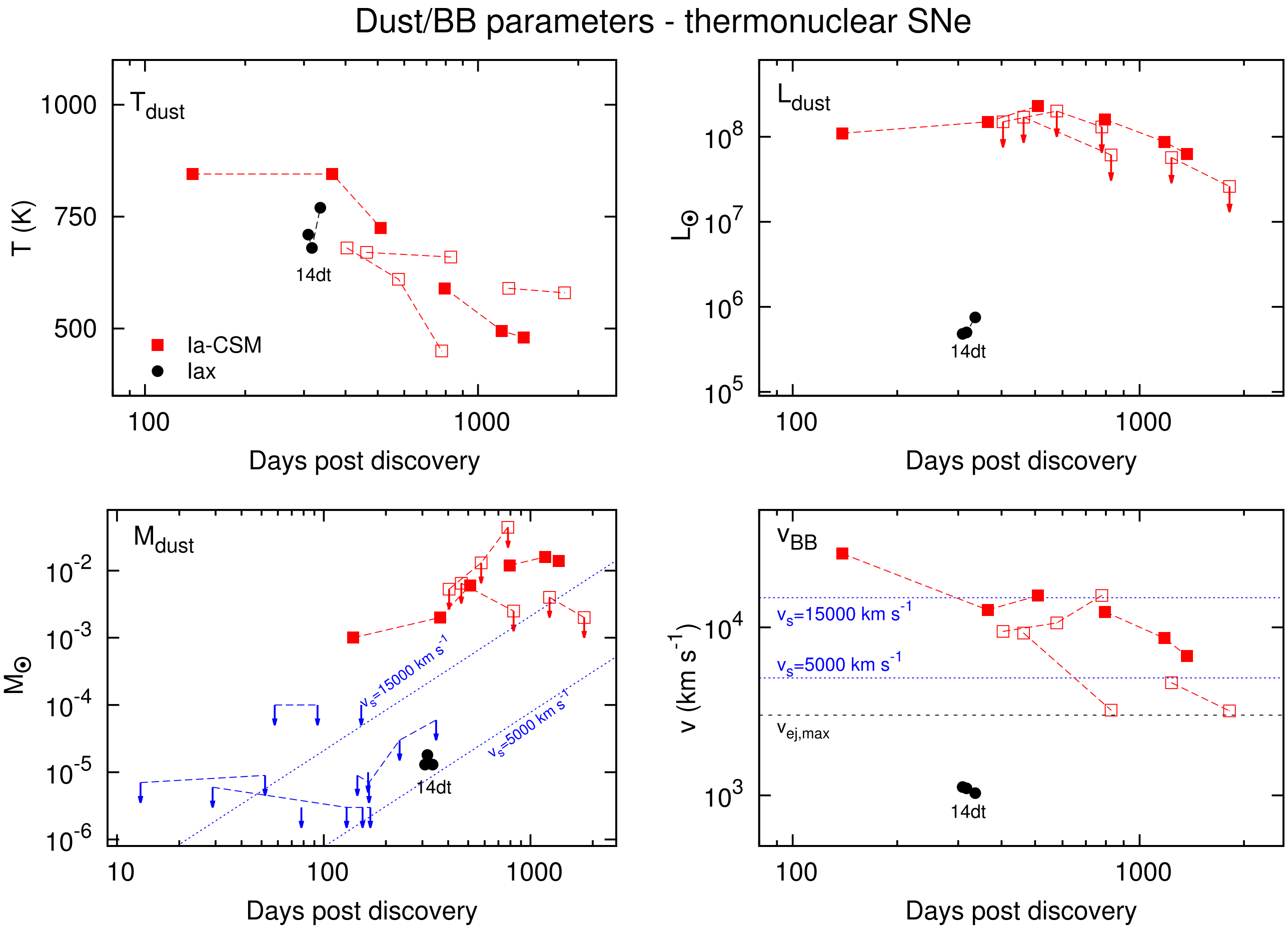

Figure 14. Dust parameters (temperatures—top left, luminosities—top right, and dust masses—bottom left) and blackbody velocities (belonging to minimum dust radii) of thermonuclear SNe derived from the SED fits. Filled and empty symbols denote SNe whose absolute magnitudes were determined with or without image subtraction, respectively. In the latter cases, only upper limits can be determined for dust masses and luminosities (marked with arrows on both bottom-left and top-right panels). Blue arrows denote upper dust mass limits for a group of SNe Ia calculated by Johansson et al. (2017). Dotted lines on the bottom-left panel denote theoretical dust masses at shock velocities $v_s = 5000$ and 15,000 km s^{-1} assuming a shock-heating scenario (see the text for details); at the bottom-right panel, the mentioned shock velocities are shown together with an upper limit of late-time ejecta velocities (black dashed line) expected in thermonuclear SNe ($v_{\rm ej,max} = 3000$ km s^{-1}; based on Silverman et al. 2013).

Tinyanont et al. 2016). Equation (2), assuming a dust-to-gas ratio of 0.01, gives the mass of dust processed by the forward shock of the SN:

$$M_{\rm d}(M_\odot) \approx 0.0028\left(\frac{v_{\rm s}}{15{,}000\ {\rm km\ s^{-1}}}\right)^3\left(\frac{t}{\rm year}\right)^2\left(\frac{a}{\mu{\rm m}}\right), \quad (2)$$

where $v_{\rm s}$ is the shock velocity, t is the time post-explosion, and a is the grain size (assumed to be 0.1 μm). The calculated dust masses—using $v_{\rm s} = 5000$ km s^{-1} and 15,000 km s^{-1} for the shock velocities assumed to be constant—appear as straight lines in the bottom-left panels of Figures 14–17. A large fraction of Type IIn and other strongly interacting SNe shows much larger dust masses than what is expected even at $v_{\rm s} = 15{,}000$ km s^{-1}; in these cases, radiative heating by the photons may emerge from the ongoing CSM interaction.

Finally, in cases where $v_{\rm BB}$ is very high (over $\sim$15,000 km s^{-1}), the dust is likely located beyond the forward shock, suggesting the dust is pre-existing at the time of the explosion and radiatively heated. Such high velocities can be seen mainly in early-time (<1 yr) observations, found, e.g., in the cases of Type IIn SN 2010jl (Fransson et al. 2014; Gall et al. 2014) or Type II-P SN 2014bi (Tinyanont et al. 2016). In these cases, another possible source of mid-IR emission may be an IR echo in which the dust shell is heated by the peak luminosity of the SN (e.g., Bode & Evans 1980; Dwek 1983; Sugerman 2003; Meikle et al. 2006). At later epochs, however, this possibility probably can be ruled out (see details in Fox et al. 2011).

4. Conclusion

Here we presented a comprehensive study of all SNe (discovered before 2015) observed with *Spitzer*/IRAC, both targeted and untargeted. In total, we increased the published sample of *Spitzer* SNe by a factor of $\sim$5× (from $\sim$200 to $\sim$1100), including nearly $\sim$2× more detections ($\sim$70 to $\sim$120).

We carry out a thorough photometric analysis of the entire SN sample, including all previously published data. In general, we find good agreements with the published values ($\lesssim$10% difference in fluxes), except in some cases that were captured in a very faint phase and/or with a complex sky background (however, for this reason, the uncertainties of their original fluxes are also implicitly large).

The results include both a detailed analysis of specific targets with unique behavior and a statistical analysis of the mid-IR

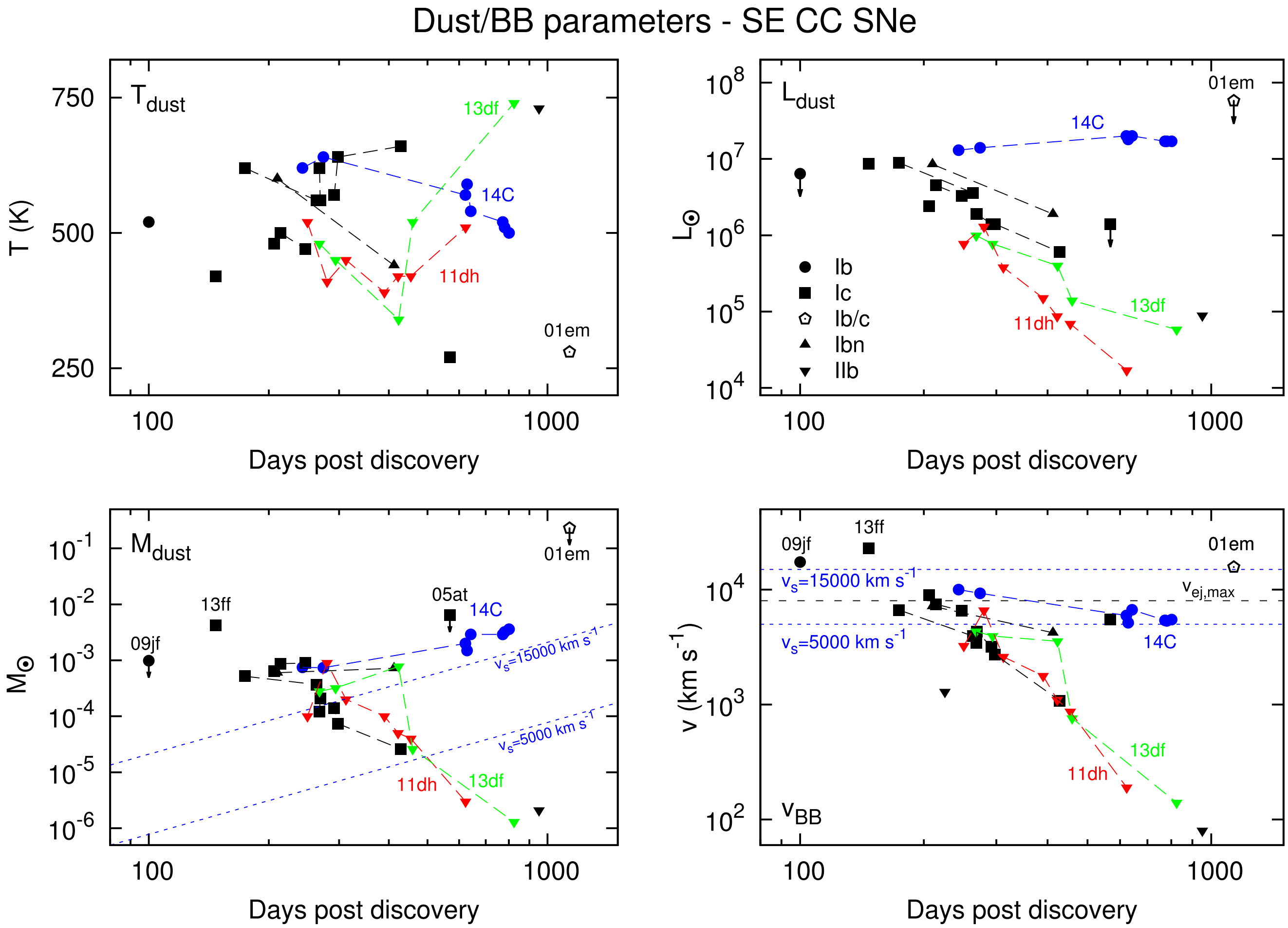

Figure 15. Same as Figure 14, except in this case for stripped-envelope CCSNe. Filled and empty symbols denote SNe whose absolute magnitudes were determined with or without image subtraction, respectively. In the latter cases (and in some other ones), only upper limits can be determined for dust masses and luminosities (marked with arrows on both bottom-left and top-right panels). At the bottom-right panel, the black dashed line denotes an upper limit of late-time ejecta velocities expected in SE CCSNe ($v_{ej,max}$ = 8000 km s^{-1}, based on Taubenberger et al. 2006).

evolution of the different SN subclasses. For each detection, we fit both BBs and simple analytic dust models. Modeling the SEDs (even in cases with just two photometry points) can disentangle the dust origin and heating mechanism, and, in some cases, determine the main physical parameters of the assumed dust. Large dust masses ($\gtrsim 10^{-3}\,M_{\odot}$) are observed primarily in Type IIn and other strongly interacting SNe. The associated v_{BB} is quite high in most of these cases, again consistent with pre-existing, radiatively heated grains.

The large data set allows us to draw some broad conclusions; nevertheless, we note that these are based on studying a quite heterogeneous sample with usually one to two epochs of data per object. In general, each subclass tends to fill its own region of phase space. Among thermonuclear explosions (looking over the late-time mid-IR data of several hundred objects, finding mostly nondetections), we see that (i) SNe Ia-CSM may be rare indeed and (ii) only a very limited number of "intermediate" cases with moderately strong CSM interaction may exist (suggested by an ∼8–10 mag gap in late-time mid-IR brightness of strongly interacting and slightly or nondetected objects). Second, in the heterogeneous group of SE CCSNe, the length of the mid-IR light curve seems to correlate with the assumed size of the progenitor (the larger the progenitor was, the longer the mid-IR light curve is, from Type eIIb SNe to Type cIIb and Type Ib/c ones); however, this finding is based on a not-so-large sample of objects. Finally, SNe IIn may remain bright for several years post-explosion or may fade more quickly.

Although this study has significantly enlarged the sample sizes for all subclasses, the cadence is quite undersampled both spectrally and temporally. Future observations with the *James Webb Space Telescope* will offer the sensitivity and spectral capabilities necessary to further constrain the dust geometry, mass, temperature, and composition.

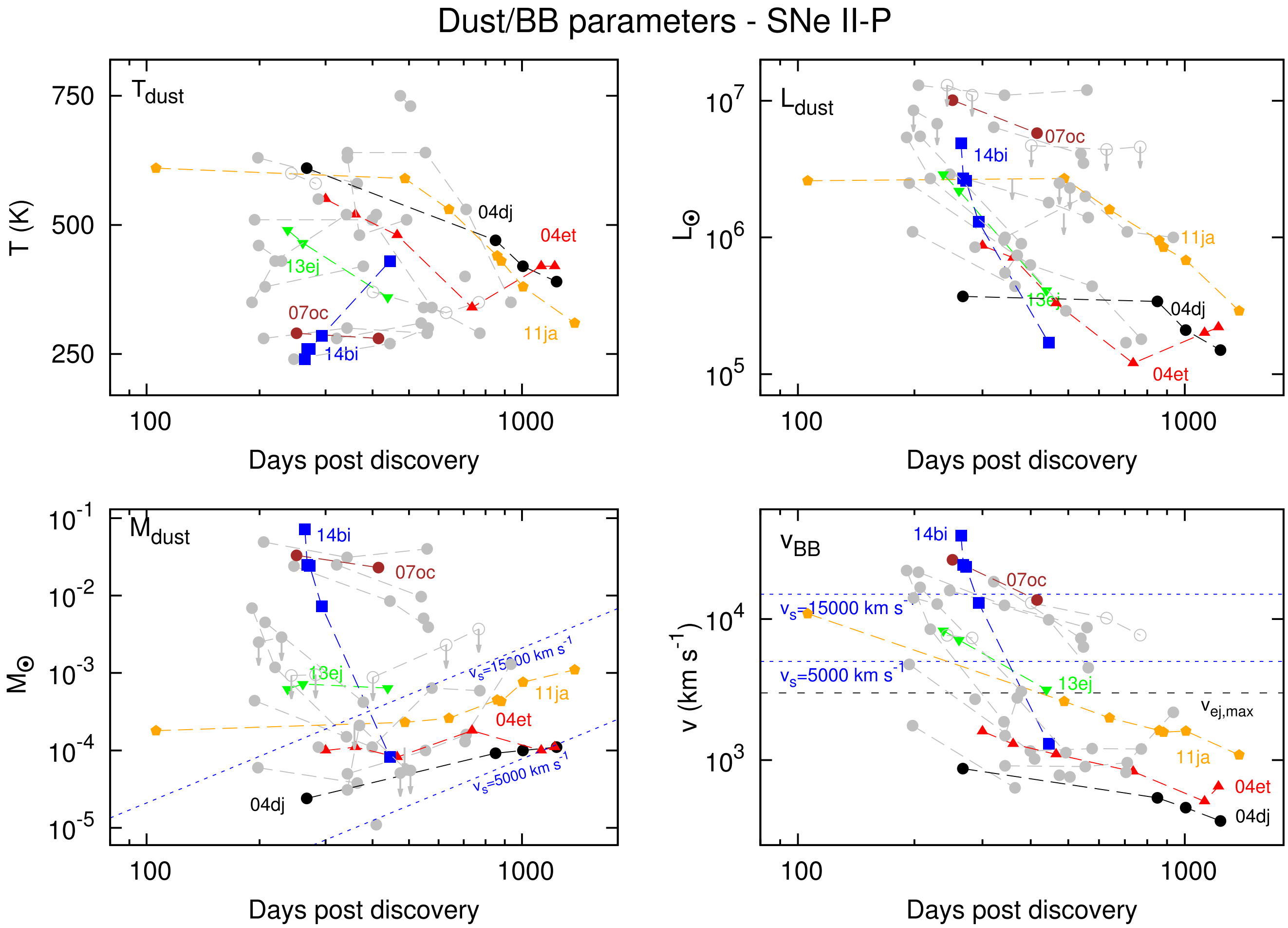

Figure 16. Same as Figure 14, except in this case for SNe II-P. Filled and empty symbols denote SNe whose absolute magnitudes were determined with or without image subtraction, respectively. In the latter cases (and in some other ones), only upper limits can be determined for dust masses and luminosities (marked with arrows on both bottom-left and top-right panels). At the bottom-right panel, the black dashed line denotes an upper limit of late-time ejecta velocities expected in SNe II-P ($v_{\rm ej,max}$ = 3000 km s^{-1}; based on Szalai et al. 2011).

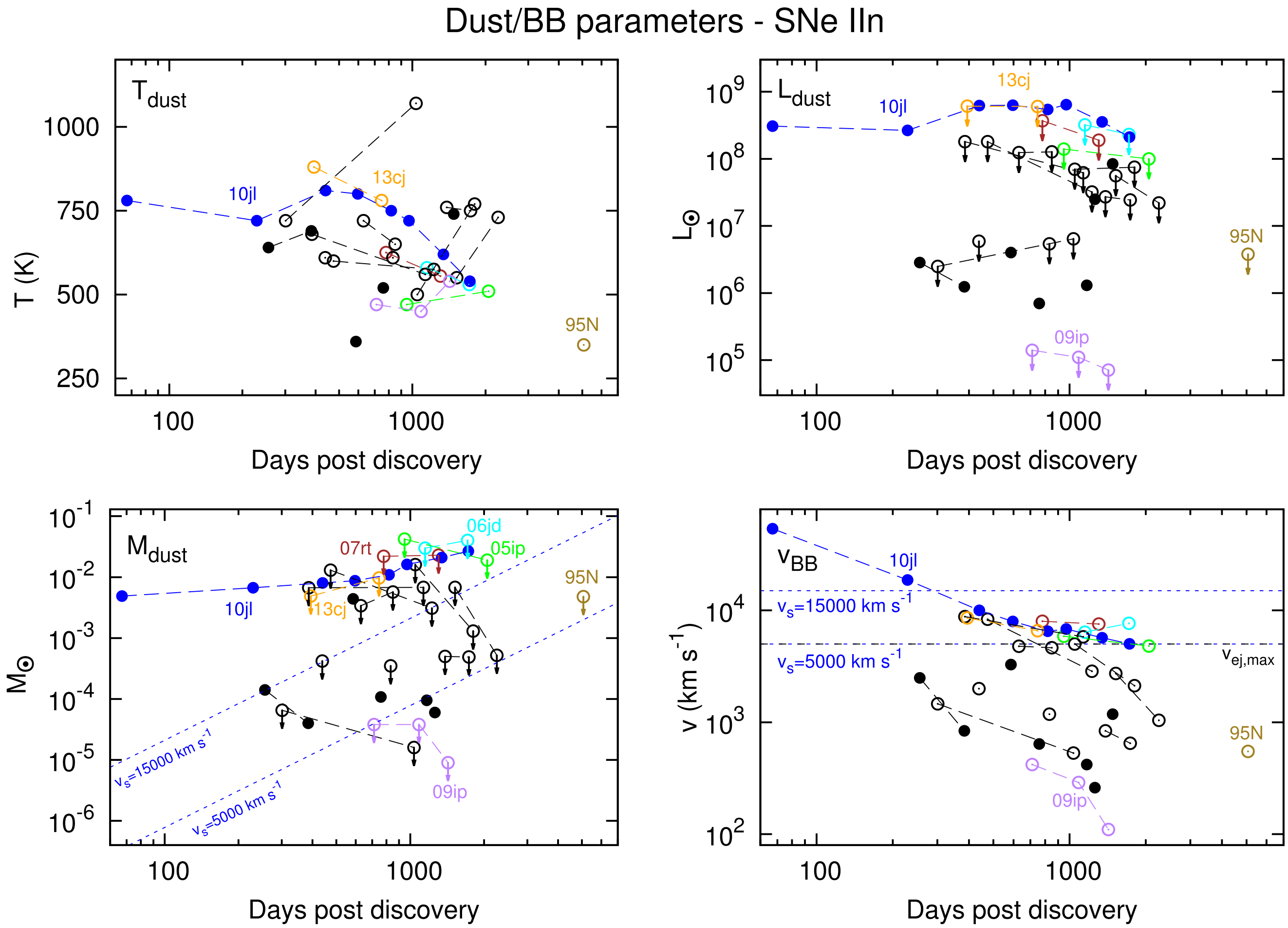

Figure 17. Same as Figure 14, except in this case for SNe IIn. Filled and empty symbols denote SNe whose absolute magnitudes were determined with or without image subtraction, respectively. In the latter cases, only upper limits can be determined for dust masses and luminosities (marked with arrows on both bottom-left and top-right panels). At the bottom-right panel, black dashed line denotes an upper limit of late-time ejecta velocities expected in SNe IIn ($v_{\mathrm{ej,max}} = 5000$ km s^{-1}; based on Patat et al. 2001).

We thank our anonymous referee for valuable comments. This work is part of the project "Transient Astrophysical Objects" GINOP-2-3-2-15-2016-00033 of the National Research, Development and Innovation Office (NKFIH), Hungary, funded by the European Union, and is also supported by the New National Excellence Program (UNKP-17-2, UNKP-17-4) of the Ministry of Human Capacities of Hungary. T.S. has received funding from the Hungarian NKFIH/OTKA PD-112325 grant. O.P. is currently supported by award PRIMUS/SCI/17 from Charles University. T.M. was supported in part by the Ministry of Economy, Development, and Tourisms Millennium Science Initiative through grant IC120009, awarded to the Millennium Institute of Astrophysics, MAS. T.M. thanks the LSSTC Data Science Fellowship Program; his time as a Fellow has benefited this work. T.M. was funded by the CONICYT PFCHA/DOCTORADO BECAS CHILE/2017-72180113.

This research has made use of the NASA/IPAC Infrared Science Archive, which is operated by the Jet Propulsion Laboratory, California Institute of Technology, under contract with the National Aeronautics and Space Administration; the NASA/IPAC Extragalactic Database (NED), which is operated by the Jet Propulsion Laboratory, California Institute of Technology, under contract with the National Aeronautics and Space Administration; and the SIMBAD database, operated at CDS, Strasbourg, France. This publication makes use of data products from the Two Micron All Sky Survey, which is a joint project of the University of Massachusetts and the Infrared Processing and Analysis Center/California Institute of Technology, funded by the National Aeronautics and Space Administration and the National Science Foundation. We acknowledge the availability of NASA ADS services.

Software: IRAF, HOTPANTS.

Appendix A
Basic Data and Mid-IR Photometry of the Studied SNe

Here, we present target details and resulting mid-IR photometry of all SNe with previously unpublished Spitzer photometry (Tables 4 and 5, respectively). We clearly highlight SNe identified on a single-epoch set of *Spitzer* images, as well as all the other SNe where image subtraction can not be applied; in all these cases, measured fluxes are strictly handled as upper limits. Additionally, Table 6 lists 3.6 and 4.5 μm absolute Vega magnitudes of all SNe positively detected by *Spitzer*/IRAC (including previously published ones). Finally, Table 7 lists the dust parameters (masses, temperatures, and mid-IR luminosities) that originate from SED fittings described in Section 3.3.

Table 4
Basic Parameters of the Studied SNe with Positive *Spitzer* Detection

Object	Type	Discovery (MJD)	Host	R.A. (J2000)	Decl. (J2000)	d (Mpc)	$E(B-V)$	References
SN 1993J	IIb	49074	NGC 3031	09:55:24.77	+69:01:13.7	3.6 ± 0.2	0.07	1
SN 1995N	IIn	49842	MCG -02-38-17	14:49:28.29	−10:10:14.0	24.0 ± 4.0	0.10	2
[a]SN 2001em	Ib/c	52172	UGC 11794	21:42:23.60	+12:29:50.3	71.6 ± 0.7	0.10	3, 4
SN 2001gd	IIb	52237	NGC 5033	13:13:23.89	+36:38:17.7	16.5 ± 7.0	0.01	5
SN 2002bu	IIn	52361	NGC 4242	12:17:37.18	+45:38:47.4	5.8 ± 1.5	0.01	6
SN 2002ed	II-P	52482	NGC 5468	14:06:38.22	−05:27:28.0	43.8 ± 7.0	0.02	7, 8
SN 2002hh	II-P	52577	NGC 6946	20:34:44.29	+60:07:19.0	5.9 ± 0.4	0.30	9
SN 2002ic	Ia-CSM	52591	A013002+2153	01:30:02.55	+21:53:06.9	280.0[b]	0.05	10
SN 2003gd	II-P	52802	NGC 628	01:36:42.65	+15:44:19.9	8.9 ± 3.2	0.06	11
SN 2003lo	IIn	53004	NGC 1376	03:37:05.12	−05:02:17.3	41.2 ± 24.0	0.04	12
SN 2004A	II-P	53011	NGC 6207	16:43:01.90	+36:50:12.5	20.3 ± 2.1	0.06	13
[a]SN 2004G	II	53023	NGC 5668	14:33:21.40	+04:26:49.5	26.9 ± 6.9	0.12	14
SN 2004W	Ia	53032	NGC 4649	12:43:36.52	+11:31:50.8	17.8 ± 0.2	0.02	15
SN 2004bv	Ia	53149	NGC 6907	20:25:06.34	−24:48:53.7	32.4 ± 6.2	0.06	16, 17
SN 2004dj	II-P	53187	NGC 2403	07:37:17.02	+65:35:57.8	3.5 ± 0.4	0.03	18
SN 2004et	II-P	53270	NGC 6946	20:35:25.33	+60:07:17.7	5.9 ± 0.4	0.30	19
SN 2005A	Ia	53375	NGC 958	02:30:43.25	−02:56:19.8	65.2 ± 10.0	0.03	20, 21
SN 2005P	Iax	53391	NGC 5468	14:06:34.01	−05:27:42.6	43.8 ± 7.0	0.03	22, 23
SN 2005W	Ia	53402	NGC 691	01:50:45.75	+21:45:35.6	36.2 ± 4.3	0.07	24, 25
SN 2005ad	II-P	53407	NGC 941	02:28:29.40	−01:08:20.0	20.8 ± 2.2	0.04	13
SN 2005af	II-P	53379	NGC 4945	13:04:44.10	−49:33:59.8	3.9 ± 0.3	0.18	13
SN 2005at	Ic	53434	NGC 6744	19:09:53.57	−63:49:22.8	9.5 ± 0.6	0.04	26
SN 2005cp	IIn	53542	UGC 12886	23:59:30.88	+18:12:09.6	127.0 ± 8.8	0.03	27
SN 2005df	Ia	53586	NGC 1559	04:17:37.85	−62:46:09.5	14.9 ± 3.6	0.03	28
SN 2005gj	Ia-CSM	53589	A030111−0033	03:01:11.96	−00:33:13.9	268.0[b]	0.10	10
SN 2005gn	IIn	53586	ESO 488−G30	05:48:49.07	−24:22:45.5	165.0[b]	0.03	27
SN 2005ip	IIn	53679	NGC 2906	09:32:06.42	+08:26:44.4	30.0 ± 7.2	0.04	27
SN 2006E	Ia	53747	NGC 5338	03:53:28.65	+05:12:22.8	12.8[b]	0.03	29, 30
SN 2006X	Ia	53770	NGC 4321	12:22:53.93	+15:48:32.0	3.6 ± 0.2	0.02	31
SN 2006bc	II-P	53819	NGC 2397	07:21:16.50	−68:59:57.3	14.7 ± 2.0	0.18	13
SN 2006bp	II-P	53834	NGC 3953	11:53:55.74	+52:21:09.4	17.5 ± 2.0	0.03	13
SN 2006ce	Ia	53865	NGC 908	02:22:54.63	−21:14:29.4	15.8 ± 2.7	0.02	32, 33
SN 2006jc	Ibn	54017	UGC 4904	09:17:20.78	+41:54:32.7	23.1 ± 5.0	0.02	34
SN 2006jd	IIn	54020	UGC 4179	08:02:07.43	+00:48:31.5	77.0 ± 5.0	0.05	27
SN 2006mq	Ia	54030	ESO 494−G26	08:06:12.39	−27:33:45.4	12.5 ± 0.6	0.36	35
SN 2006my	II-P	53953	NGC 4651	12:43:40.70	+16:23:14.1	22.3 ± 2.2	0.03	13
SN 2006ov	II-P	53964	NGC 4303	12:21:55.30	+04:29:16.7	12.6 ± 1.2	0.02	13
SN 2006qq	IIn	54069	ESO 553−G36	05:19:50.30	−20:58:06.4	119.0 ± 5.0	0.02	27
SN 2007af	Ia	54160	NGC 5584	14:22:21.03	−00:23:37.6	22.1 ± 5.6	0.03	31
SN 2007gr	Ic	54327	NGC 1058	02:43:27.98	+37:20:44.7	9.3 ± 1.2	0.05	36
SN 2007it	II-P	54356	NGC 5530	14:18:25.63	−43:22:53.8	11.9 ± 1.5	0.10	37
SN 2007le	Ia	54386	NGC 7721	23:38:48.45	−06:31:21.7	22.2 ± 3.2	0.03	31
SN 2007oc	II-P	54408	NGC 7418A	22:56:41.8	−36:46:22.3	28.0 ± 3.2	0.02	13
SN 2007od	II-P	54406	UGC 12846	23:55:48.68	+18:24:54.8	26.7 ± 3.2	0.03	38
SN 2007rt	IIn	54423	UGC 6109	11:02:34.29	+50:34:58.5	93.0 ± 8.0	0.01	27
SN 2007sq	II-P	54442	MCG -03-23-05	08:47:16.13	−20:01:27.6	72.7 ± 10.7	0.18	39
SN 2007 sr	Ia	54452	NGC 4038	12:01:52.80	−18:58:21.7	21.5 ± 4.2	0.04	31
SN 2008J	IIn	54480	MCG -02-07-33	02:34:24.20	−10:50:38.5	66.0 ± 5.0	0.02	27
SN 2008Q	Ia	54491	NGC 524	01:24:57.23	+09:33:01.5	26.4 ± 4.2	0.07	31
SN 2008cg	IIn	54591	PGC 91487	15:54:15.15	+10:58:25.0	122.0[b]	0.05	27
SN 2008en	IIn	54681	UGC 564	00:55:13.56	+35:26:26.2	151.0 ± 5.0	0.04	27
SN 2008fq	II	54724	NGC 6907	20:25:06.19	−24:48:27.6	32.4 ± 6.2	0.06	40, 41
SN 2008gm	IIn	54761	NGC 7530	23:14:12.39	−02:46:52.4	48.0 ± 3.5	0.04	27
SN 2008ip	IIn	54650	NGC 4846	12:57:50.20	+36:22:33.5	63.0 ± 5.0	0.01	27
SN 2008jb	II	54789	ESO 302−G13	03:51:44.66	−38:27:00.1	9.6 ± 3.0	0.01	42
SN 2009E	II-P	54834	NGC 4141	12:09:49.56	+58:50:50.3	37.5[b]	0.02	43, 44
SN 2009H	II	54833	NGC 1084	02:45:58.36	−07:35:00.3	17.5 ± 1.0	0.03	45, 46
SN 2009af	II	54878	UGC 1551	02:03:36.37	+24:04:40.9	35.6[b]	0.08	47, 48
SN 2009at	II	54901	NGC 5301	13:46:26.68	+46:06:09.1	23.0 ± 2.3	0.02	49, 50
SN 2009em	Ic	54956	NGC 157	00:34:44.53	−08:23:57.6	16.8 ± 5.0	0.04	51, 52
SN 2009gj	IIb	55002	NGC 134	00:30:28.56	−33:12:56.0	17.1 ± 3.2	0.02	53, 54
SN 2009ig	Ia	55063	NGC 1015	02:38:11.62	−01:18:45.3	36.6 ± 1.5	0.03	31
SN 2009ip	IIn	56193	NGC 7259	22:23:08.3	−28:56:52	20.5 ± 2.0	0.02	27
[a]SN 2009iu	Ib	55075	NGC 7329	22:40:10.35	−66:28:06.4	44.3 ± 5.7	0.03	55, 56
SN 2009jf	Ib	55101	NGC 7479	23:04:52.98	+12:19:59.5	29.3 ± 6.1	0.10	57, 58
SN 2009jr	Ia	55112	IC 1320	20:26:26.03	+02:54:32.1	70.0 ± 5.0[b]	0.12	59, 60
SN 2009js	II-P p.	55115	NGC 918	02:25:48.28	+18:29:25.8	17.9 ± 6.2	0.31	61
SN 2009mk	IIb	55180	ESO 293−34	00:06:21.37	−41:28:59.8	20.0 ± 1.5	0.02	62, 63
SN 2010B	Ia	55203	NGC 5370	13:54:08.74	+60:40:50.4	43.0 ± 3.2	0.02	64, 65
SN 2010F	II	55209	NGC 3120	10:05:21.05	−34:13:21.0	32.2 ± 7.6	0.09	66, 67
SN 2010gp	Ia	55391	NGC 6240	16:52:57.39	+02:23:16.4	100.0 ± 7.5[b]	0.07	68, 69

Table 4
(Continued)

Object	Type	Discovery (MJD)	Host	R.A. (J2000)	Decl. (J2000)	d (Mpc)	$E(B-V)$	References
SN 2010jl	IIn	55503	UGC 5189A	09:42:53.33	+09:29:41.8	48.9 ± 3.4	0.02	70
SN 2010mc	IIn	55428	A172130+4807	17:21:30.68	+48:07:47.4	159.0[b]	0.02	71, 72
SN 2011A	IIn	55563	NGC 4902	13:01:01.19	−14:31:34.8	33.8 ± 3.5	0.04	73, 74
SN 2011ae	Ia	55604	MCG -03-30-19	11:54:49.25	−16:51:43.6	27.5[b]	0.05	75, 76
SN 2011dh	IIb	55713	NGC 5194	13:30:05.11	+47:10:10.9	7.7 ± 0.5	0.02	77
SN 2011dq	II	55696	NGC 337	00:59:47.75	−07:34:20.5	20.7 ± 2.6	0.10	78
SN 2011dx	Ia-pec.	55739	NGC 1376	03:37:05.61	−05:01:56.3	60.8 ± 3.0	0.04	79, 80
SN 2011fe	Ia	55816	NGC 5457	14:03:05.71	+54:16:25.2	6.1 ± 0.5	0.01	31
SN 2011fh	IIn	55797	NGC 4806	12:56:14.01	−29:29:54.82	33.3 ± 2.6[b]	0.04	81, 82
[a]SN 2011ft	Ib	55803	UGC 11021	17:52:42.98	+29:04:10.6	101.0 ± 3.0	0.06	83, 84
SN 2011ht	IIn	55833	UGC 5460	10:08:10.56	+51:50:57.12	17.8 ± 3.0	0.01	85, 86
[a]SN 2011ir	IIn	55886	UGC 6771	11:48:00.32	+04:29:47.1	70.3 ± 11.6	0.02	87
SN 2011iy	Ia	55904	NGC 4984	13:08:58.39	−15:31:04.1	21.3 ± 2.1	0.06	88, 89
SN 2011ja	II-P	55906	NGC 4945	13:05:11.12	−49:31:27.0	3.8 ± 0.5	0.15	90
PTF11kx	Ia-CSM	55579	anon.	08:09:12.87	+46:18:48.8	200.0[b]	0.04	91
PTF11qcj	Ic	55840	anon.	13:13:41.51	+47:17:57.0	125.0[b]	0.01	92
SN 2012aw	II-P	56002	NGC 3351	10:43:53.73	+11:40:17.6	8.8 ± 1.1	0.02	93
SN 2012ca	Ia-CSM	56042	ESO 336−09	18:41:07.25	−41:47:38.4	80.0 ± 6.0[b]	0.07	94, 95
[a]SN 2012cd	IIb	56053	MCG +09-22-53	13:22:35.25	+54:48:47.7	50.0 ± 3.7[b]	0.03	96, 97
SN 2012cg	Ia	56082	NGC 4424	12:27:12.83	+09:25:13.2	7.3 ± 0.5	0.02	31
SN 2012fh	Ic	56218	NGC 3344	10:43:34.05	+24:53:29.0	9.8 ± 2.5	0.03	98
[a]SN 2013E	Ia	56296	IC 2532	10:00:05.52	−34:14:01.3	27.2 ± 6.8	0.09	99
SN 2013L	IIn	56314	ESO 216−G39	11:45:29.55	−50:35:53.1	75.0 ± 5.0[b]	0.11	35
SN 2013ai	II	56352	NGC 2207	06:16:18.35	−21:22:32.9	14.3 ± 2.0	0.08	35
SN 2013am	II	56372	NGC 3623	11:18:56.95	+13:03:49.4	18.5 ± 2.2	0.02	35
SN 2013bu	II	56403	NGC 7331	22:37:02.17	+34:24:05.2	13.1 ± 1.5	0.08	35
SN 2013cj	IIn	56421	UGC 10685	17:04:52.95	+12:55:10.4	135.0 ± 10.0[b]	0.09	100
SN 2013df	IIb	56447	NGC 4414	12:26:29.33	+31:13:38.3	16.6 ± 0.4	0.02	101
SN 2013dk	Ic	56465	NGC 4038	12:01:52.72	−18:52:18.3	21.5 ± 4.2	0.04	35
SN 2013dn	Ia-CSM	56457	PGC 71942	23:37:45.74	+14:42:37.1	230.0[b]	0.07	102
SN 2013dy	Ia	56483	NGC 7250	22:18:17.60	+40:34:09.6	13.7 ± 4.4	0.13	103
SN 2013ee	II	56486	NGC 3079	10:01:56.83	+55:41:44.0	14.9 ± 4.0	0.01	104
SN 2013ej	II-P/L	56497	NGC 628	01:36:48.16	+15:45:31.0	9.5 ± 0.6	0.06	105
SN 2013ff	Ic	56535	NGC 2748	09:13:38.88	+76:28:10.8	20.2 ± 2.8	0.03	106
SN 2014C	Ib	56662	NGC 7331	22:37:05.60	+34:24:31.9	13.1 ± 1.0	0.08	35
SN 2014G	II-L	56671	NGC 3448	10:54:34.13	+54:17:56.9	24.5[b]	0.01	107, 108
SN 2014J	Ia	56677	NGC 3034	09:55:42.12	+69:40:25.9	3.3 ± 0.2	0.14	31
SN 2014L	Ic	56683	NGC 4254	12:18:48.68	+14:24:43.5	16.8 ± 1.2	0.03	35
SN 2014bi	II-P	56809	NGC 4096	12:06:02.99	+47:29:33.5	11.6 ± 2.5	0.02	35
SN 2014cx	II-P	56902	NGC 337	00:59:47.83	−07:34:18.6	19.6 ± 2.6	0.11	109, 110
SN 2014df	Ib	56811	NGC 1448	03:44:23.99	−44:40:08.1	13.4 ± 2.0	0.01	35
SN 2014dt	Iax	56950	NGC 4303	12:21:57.57	+04:28:18.5	18.7 ± 7.3	0.02	111

Notes.
[a] Positive detection based on single-epoch imaging; see the text for details.
[b] Distance calculated from redshift.

References. (1) Filippenko et al. (1993), (2) Van Dyk (2013), (3) Papenkova et al. (2001), (4) Bietenholz & Bartel (2005), (5) Matheson et al. (2001), (6) Szczygiel et al. (2012), (7) Monard & Li (2002), (8) Salvo & Price (2002), (9) Meikle et al. (2006), (10) Fox & Filippenko (2013), (11) Sugerman et al. (2006), (12) Meikle et al. (2005), (13) Szalai & Vinkó (2013), (14) Nakano et al. (2004b), (15) Moore et al. (2004), (16) Nakano et al. (2004a), (17) Li et al. (2004), (18) Szalai et al. (2011), (19) Kotak et al. (2009), (20) Graham & Li (2005), (21) Modjaz et al. (2005), (22) Burket & Li (2005), (23) Jha et al. (2006), (24) Nakano et al. (2005), (25) Elias-Rosa et al. (2005), (26) Kankare et al. (2014), (27) Fox et al. (2011), (28) Gerardy et al. (2007), (29) Puckett et al. (2006), (30) Aldering et al. (2006); (31) Johansson et al. (2017), (32) Ponticello et al. (2006), (33) Blackman et al. (2006), (34) Mattila et al. (2008), (35) Tinyanont et al. (2016), (36) Kochanek et al. (2011), (37) Andrews et al. (2011b), (38) Andrews et al. (2010), (39) Lennarz et al. (2012), (40) Thrasher et al. (2008); (41) Quinn et al. (2008), (42) Prieto et al. (2012), (43) Boles (2009), (44) Navasardyan et al. (2009), (45) Li et al. (2009a), (46) Benetti et al. (2009), (47) Cortini (2009), (48) Ciroi et al. (2009), (49) Nakano et al. (2009), (50) Harutyunyan et al. (2009), (51) Monard (2009), (52) Navasardyan & Benetti (2009), (53) Marples et al. (2009), (54) Foley (2009), (55) Maza et al. (2009), (56) Morrell & Phillips (2009), (57) Li et al. (2009b), (58) Kasliwal et al. (2009), (59) Arbour & Briggs (2009), (60) Silverman et al. (2009), (61) Gandhi et al. (2013), (62) Marples & Drescher (2009), (63) Chornock & Berger (2009), (64) Nakano et al. (2010), (65) Kasliwal (2010), (66) Maza et al. (2010a), (67) Foley (2010), (68) Maza et al. (2010b), (69) Folatelli et al. (2010), (70) Fox et al. (2013), (71) Howell & Murray (2010), (72) Ofek et al. (2013), (73) Pignata et al. (2011), (74) Stritzinger et al. (2011), (75) Howerton et al. (2011), (76) Sahu et al. (2011a), (77) Helou et al. (2013), (78) Monard et al. (2011b), (79) Monard & Prieto (2011), (80) Prieto (2011a), (81) Monard et al. (2011a), (82) Prieto & Seth (2011), (83) Balanutsa et al. (2011), (84) Prieto (2011b), (85) Boles (2011), (86) Prieto et al. (2011), (87) Tomasella et al. (2011), (88) Itagaki et al. (2011), (89) Chen et al. (2011), (90) Andrews et al. (2016), (91) Graham et al. (2017), (92) Corsi et al. (2014), (93) Siviero et al. (2012), (94) Drescher et al. (2012), (95) Valenti et al. (2012), (96) Shurpakov et al. (2012), (97) Marion et al. (2012), (98) Nakano et al. (2012), (99) Morrell et al. (2006), (100) Jin et al. (2013), (101) Szalai et al. (2016), (102) Drake et al. (2013), (103) Casper et al. (2013), (104) Cortini et al. (2013), (105) Mauerhan et al. (2017), (106) Brimacombe et al. (2013), (107) Ochner et al. (2014), (108) Zheng et al. (2014), (109) Holoien et al. (2014), (110) Andrews et al. (2015), (111) Fox et al. (2016).

(This table is available in machine-readable form.)

Table 5
Mid-IR Fluxes of SNe with Previously Unreported *Spitzer* Photometry

Object	Type	MJD−2,450,000	Epoch[†] (days)	$F_{\nu,[3.6]}$ (μJy)	$F_{\nu,[4.5]}$ (μJy)	$F_{\nu,[5.8]}$ (μJy)	$F_{\nu,[8.0]}$ (μJy)	SN-targeted observation?
*SN 2001em[a]	Ib/c	53307[e]	1135	303(41)	349(36)	481(50)	859(105)	Yes
SN 2001gd[b]	IIb	53189[f]	952	11(8)	12(7)	non[‡]	non[‡]	No
SN 2002ed[c]	II-P	53569[g]	1086	non[‡]	7(7)	non[‡]	non[‡]	No
*SN 2004G[a]	II	53047[h]	24	249(28)	395(33)	265(30)	196(29)	No
SN 2004W[a,b]	Ia	53166[h]	134	non[‡]	non[‡]	non[‡]	212(29)	No
SN 2004bv[b]	Ia	53308[i]	159	22(17)	non[‡]	non[‡]	non[‡]	No
SN 2005A[a,b]	Ia	53387[i]	12	154(112)	64(64)	non[‡]	non[‡]	No
SN 2005P[b]	Iax	53569[g]	178	non[‡]	non[‡]	non[‡]	54(32)	Yes
SN 2005W[a,b]	Ia	53607[g]	205	8(8)	5(5)	non[‡]	177(28)	Yes
		53770[g]	368	non[‡]	non[‡]	non[‡]	128(24)	Yes
SN 2006E[a,b]	Ia	53955[k]	208	30(10)	17(7)	14(8)	233(29)	Yes
		54150[k]	403	non[‡]	non[‡]	21(8)	54(14)	Yes
*SN 2006F[a]	Ib	53770[l]	24	400(43)	301(34)	non[‡]	non[‡]	No
SN 2006ce[a,b]	Ia	53955[k]	90	146(21)	38(10)	29(9)	511(42)	No
		54355[m]	490	non[‡]	non[‡]	non[‡]	65(15)	No
SN 2007sq[b]	II-P	54596[n]	154	224(35)	…	330(45)	non[‡]	No
SN 2008fq[c]	II	55892[o]	1168	40(40)	55(45)	…	…	No
SN 2009E[c]	II-P	55381[p]	547	10(10)	37(13)	…	…	No
SN 2009H[a]	II	55077[j]	243	1312(104)	1929(96)	…	…	No
		55116[j]	282	1044(100)	1672(88)	…	…	No
SN 2009af[a]	II	55077[p]	199	125(20)	265(27)	…	…	No
		55107[q]	229	79(15)	188(23)	…	…	No
SN 2009at[a]	II	55375[r]	474	161(34)	172(28)	…	…	No
		55406[r]	505	150(34)	165(28)	…	…	No
SN 2009em[b]	Ic	55073[s]	117	65(26)	232(32)	…	…	No
SN 2009gj[a,b]	IIb	55070[s]	68	244(26)	450(35)	…	…	No
*SN 2009iu[a]	Ib	55142[t]	67	149(20)	227(25)	…	…	No
SN 2009jf[c]	Ib	55201[u]	100	180(25)	307(31)	…	…	No
SN 2009jr[b]	Ia	55150[v]	38	54(54)	non[‡]	…	…	Yes
		55161[v]	49	45(45)	non[‡]	…	…	Yes
		55171[v]	59	23(23)	non[‡]	…	…	Yes
SN 2009mk[c]	IIb	55405[p]	225	75(35)	107(31)	…	…	No
SN 2010B[a]	Ia	55246[v]	43	111(18)	45(11)	…	…	Yes
		55281[v]	78	73(15)	31(9)	…	…	Yes
		55311[v]	108	61(14)	29(9)	…	…	Yes
		55343[i]	140	59(13)	33(10)	…	…	Yes
SN 2010F[b]	II	55416[x]	207	41(16)	120(21)	…	…	Yes
		55587[x]	378	10(10)	25(12)	…	…	Yes
		55740[y]	531	non[‡]	5(5)	…	…	Yes
SN 2010gp[c]	Ia	55498[z]	107	12(8)	8(6)	…	…	No
SN 2010mc[a]	IIn	56814[ε]	1386	35(9)	38(10)	…	…	Yes
		57163[w]	1735	32(9)	34(10)	…	…	Yes
SN 2011A[a,c]	IIn	55649[α]	86	58(13)	49(12)	…	…	No
SN 2011ae[a,c]	Ia	55616[β]	12	1037(55)	724(46)	…	…	No
SN 2011dq[c]	II	56955[γ]	1259	1230(61)	963(55)	…	…	No
SN 2011dx[c]	Ia-pec.	55864[δ]	125	7(6)	non[‡]	…	…	No
SN 2011fh[a,c]	IIn	56383[ε]	586	23(18)	59(20)	…	…	Yes
*SN 2011ft[a]	Ib	56060[j]	257	81(15)	…	…	…	No
SN 2011ht[a,b]	IIn	55833[ζ]	638	non[‡]	8(4)	…	…	Yes
*SN 2011ir[a]	IIn	55886[ζ]	832	35(10)	47(11)	…	…	Yes
SN 2011iy[c]	Ia	56932[γ]	1028	…	5(5)	…	…	No
SN 2012aw[c,d]	II-P	56360[φ]	358	135(14)	521(35)	…	…	Yes
		56489[φ]	487	38(10)	166(20)	…	…	Yes
		56700[ι]	698	5(5)	13(5)	…	…	Yes
SN 2012ca[a,d]	Ia-CSM	56446[ζ]	404	812(86)	963(74)	…	…	Yes
		56619[ζ]	577	999(90)	1362(80)	…	…	Yes
		56820[ζ]	778	328(77)	716(67)	…	…	Yes
*SN 2012cd[a]	IIb	56090[η]	37	297(28)	306(29)	…	…	No
SN 2012fh[a,c]	Ic	56117[κ]	8	3324(96)	2756(88)	…	…	No
		56122[κ]	13	3640(102)	2903(92)	…	…	No
		56323[μ]	214	1058(55)	1916(74)	…	…	Yes
		56356[μ]	247	649(44)	1292(61)	…	…	Yes
		56692[ι]	583	non[‡]	16(5)	…	…	Yes

Table 5
(Continued)

Object	Type	MJD−2,450,000	Epoch[†] (days)	$F_{\nu,[3.6]}$ (μJy)	$F_{\nu,[4.5]}$ (μJy)	$F_{\nu,[5.8]}$ (μJy)	$F_{\nu,[8.0]}$ (μJy)	SN-targeted observation?
[*]SN 2013E[a]	*Ia*	*56376[j]*	*80*	*111(18)*	⋯	⋯	⋯	*No*
SN 2013cj[a]	*IIn*	*56815[ε]*	*394*	*998(52)*	*916(51)*	⋯	⋯	*Yes*
		57168[w]	*747*	*1097(56)*	*1120(57)*	⋯	⋯	*Yes*
SN 2013dn[a,d]	*Ia-CSM*	*56920[ε]*	*463*	*107(19)*	*131(20)*	⋯	⋯	*Yes*
		57285[w]	*828*	*38(11)*	*47(12)*	⋯	⋯	*Yes*
SN 2013dy[b]	Ia	56691[ϑ]	208	34(19)	7(7)	⋯	⋯	Yes
		56731[ι]	248	18(19)	7(7)	⋯	⋯	Yes
SN 2013ee[a,b]	II	56677[ι]	191	120(40)	417(35)	⋯	⋯	Yes
		56706[ι]	220	171(40)	393(35)	⋯	⋯	Yes
		56827[ι]	341	106(40)	178(35)	⋯	⋯	Yes
		57057[ν]	571	9(5)	13(5)	⋯	⋯	Yes
SN 2013ff[c]	Ic	56682[γ]	147	263(66)	632(59)	⋯	⋯	No
SN 2014G[c]	II-L	57232[w]	561	41(15)	85(17)	⋯	⋯	Yes
SN 2014cx[c]	II-P	56955[γ]	53	1312(60)	992(53)	⋯	⋯	No

Note. Photometric methods: [a]aperture photometry on the original images; [b]ap. photometry after subtracting a very late-time image + flux differences; [c]ap. photometry after subtracting a pre-explosion image + flux differences; [d] "Fox+11 method" (see details in the text). [*]Positive detection based on single-epoch imaging. Data marked with italics denote cases where image subtraction cannot be applied (in all these cases, measured fluxes can be handled only as upper limits). Program IDs: [e]3641 (PI van Dyk); [f]159 (PI Kennicutt); [g]20256 (PI Meikle); [h]69 (PI Fazio); [i]3672 (PI Mazzarella); [j]80072 (PI Tully); [k]30292 (PI Meikle); [l]20140 (PI Zezas); [m]40619 (PI Kotak); [n]50111 (PI McGaugh); [o]80089 (PI Sanders); [p]61060 (PI Sheth); [q]30496 (PI Fisher); [r]80254 (PI Stern); [s]61065 (PI Sheth); [t]61003 (PI Freedman); [u]61009 (PI Freedman); [v]60166 (PI Garnavich); [w]11053 (PI Fox); [x]70008 (PI Andrews); [y]80131 (PI Andrews); [z]70038 (PI Sanders); [ε]10139 (PI Fox); [ζ]90137 (PI Fox); [α]61066 (PI Sheth); [β]61062 (PI Sheth); [γ]10046 (PI Sanders); [δ]80023 (PI Fox); [φ]90178 (PI Andrews); [η]80069 (PI Beygu); [ϑ]10152 (PI Kasliwal); [ι]10136 (PI Kasliwal); [κ]800025 (PI van Zee); [μ]80196 (PI Kasliwal); [ν]11063 (PI Kasliwal). Additional notes: [†]Days since discovery; [‡]No point source at the position of the SN.

(This table is available in machine-readable form.)

Table 6
3.6 and 4.5 μm Absolute Vega Magnitudes of all SNe Positively Detected by *Spitzer*/IRAC

Object	Type	MJD−2,450,000	Epoch (days)	Absolute mag. 3.6 μm	Absolute mag. 4.5 μm	Source of Data[a]
SN 1993J	IIb	52948	3874	−11.67(0.10)	−12.79(0.10)	1
		52976	3902	−11.85(0.15)	−12.93(0.10)	1
		53125	4051	−11.48(0.10)	−12.55(0.10)	1
		53357	4283	−11.55(0.10)	−12.62(0.10)	1
		53497	4423	−11.71(0.10)	−12.58(0.10)	1
		53665	4591	−11.40(0.10)	−12.47(0.10)	1
		54419	5345	−11.15(0.10)	−12.00(0.10)	1
		55736	6662	−10.55(0.25)	−10.93(0.25)	1
		55936	6862	−10.88(0.25)	−11.29(0.25)	1
		56671	7597	−10.78(0.25)	−11.15(0.25)	1
		56699	7625	−10.45(0.25)	−10.92(0.25)	1
		56820	7746	−10.45(0.25)	−10.71(0.25)	1
SN 1995N	*IIn*	*54909*	*5067*	*−15.21(0.44)*	*−16.51(0.39)*	*2*
SN 2001em	*Ib/c*	*53307*	*1135*	*−19.37(0.15)*	*−20.00(0.11)*	*This work*
SN 2001gd	IIb	53189	952	−12.59(1.00)	−13.28(1.00)	This work
SN 2002bu	IIn	53120	759	−14.52(0.56)	−15.47(0.56)	3
SN 2002ed	II-P	53569	1086	non	−14.68(1.14)	This work
SN 2002hh	II-P	53167	590	non	−14.13(0.51)	4
		53261	684	non	−14.19(0.51)	4
		53335	758	non	−13.12(0.98)	4
SN 2002ic	Ia-CSM	53386	795	−20.63(0.18)	−21.51(0.19)	5
		53770	1179	−19.66(0.23)	−20.66(0.20)	5
		53961	1370	−19.26(0.24)	−20.29(0.24)	5
SN 2003gd	II-P	53211	409	−11.89(0.92)	−13.74(0.81)	6
		53385	583	non	−10.96(1.26)	6
SN 2003lo	IIn	53260	256	−17.63(0.34)	−18.37(0.27)	7
		53388	384	−16.76(0.58)	−17.40(0.43)	7
		53771	767	non	−15.49(1.09)	7
SN 2004A	II-P	53258	247	−15.65(0.47)	−16.50(0.46)	8
		53456	445	−14.73(0.49)	−15.05(0.49)	8
		53574	563	−14.43(0.54)	−14.67(0.56)	8
SN 2004G	*II*	*53047*	*24*	*−17.03(0.57)*	*−18.01(0.56)*	*This work*
SN 2004bv	Ia	53308	159	−14.80(0.48)	non	This work
SN 2004dj	II-P	53285	98	−16.69(0.37)	−17.02(0.37)	9
		53286	99	−16.66(0.37)	−17.03(0.37)	9
		53290	103	−16.36(0.37)	−17.00(0.37)	9
		53310	123	−15.67(0.37)	−16.75(0.37)	9
		53454	267	−14.30(0.37)	−15.89(0.37)	9
		53663	476	−14.74(0.37)	−15.45(0.37)	9
		53818	631	−14.39(0.37)	−15.13(0.37)	9
		54037	850	−13.88(0.37)	−14.68(0.37)	9
		54040	853	−13.87(0.37)	−14.66(0.37)	9
		54193	1006	−13.28(0.37)	−14.07(0.37)	9
		54424	1237	−12.93(0.37)	−13.64(0.37)	9
		54428	1241	−12.92(0.37)	−13.63(0.37)	9
		54429	1242	−12.94(0.37)	−13.64(0.37)	9
		54564	1377	−12.85(0.37)	−13.45(0.37)	9
		54569	1382	−12.84(0.37)	−13.46(0.37)	10
SN 2004et	II-P	53335	65	−18.38(0.15)	−18.53(0.14)	11
		53571	300	−14.93(0.15)	−16.98(0.14)	11
		53631	360	−14.36(0.14)	−16.33(0.14)	11
		53676	406	−14.02(0.15)	−15.79(0.14)	11
		53735	465	−13.37(0.16)	−15.28(0.15)	11
		53960	690	non	−12.39(0.38)	11
		54006	736	non	−12.04(0.51)	11
		54065	795	non	−11.59(0.20)	11
		54098	828	non	−12.19(0.17)	11
		54285	1015	non	−11.54(0.21)	11
		54396	1125	−12.32(0.16)	−13.94(0.15)	11
		54461	1191	−12.09(0.17)	−13.98(0.15)	11
		54493	1222	−12.11(0.17)	−14.09(0.15)	11
		54665	1395	−12.47(0.34)	−14.27(0.15)	12
		55049	1779	−10.85(0.53)	−13.37(0.16)	12

Table 6
(Continued)

Object	Type	MJD−2,450,000	Epoch (days)	Absolute mag. 3.6 μm	Absolute mag. 4.5 μm	Source of Data[a]
		55201	1931	−10.64(0.56)	−13.12(0.25)	12
		55421	2151	non	−12.95(0.16)	12
SN 2005A	Ia	53387	12	−18.42(0.35)	−17.95(0.35)	This work
SN 2005W	Ia	53607	205	−13.94(0.56)	−14.01(0.77)	This work
SN 2005ad	II-P	53605	198	−15.32(0.83)	−15.96(0.83)	8
		53771	364	−14.19(0.87)	−15.30(0.85)	8
SN 2005af	II-P	53573	194	−15.82(0.27)	−17.97(0.27)	8
		53779	399	−14.31(0.27)	−16.14(0.27)	8
		53955	576	−12.87(0.29)	−14.06(0.29)	8
		54151	772	−12.19(0.30)	−12.45(0.31)	8
		54320	940	non	−12.25(0.30)	8
SN 2005at	Ic	54003	569	−13.02(0.39)	−13.85(0.30)	13
SN 2005cp	*IIn*	*55065*	*1523*	*−20.53(0.19)*	*−21.10(0.18)*	*14*
		55796	*2254*	*−20.23(0.21)*	*−20.51(0.20)*	*15*
		56542	*3000*	*−20.14(0.21)*	*−20.28(0.20)*	*This work*
SN 2005df	Ia	53676	90	−15.99(0.53)	−14.72(0.57)	16
		53773	187	−14.34(0.57)	−13.41(0.68)	16
		53955	369	−12.66(0.74)	−12.35(0.90)	16
SN 2005gj	Ia-CSM	53778	139	−20.40(0.19)	−20.99(0.20)	5
		54004	365	−20.73(0.18)	−21.18(0.19)	5
		54149	510	−21.22(0.19)	−21.83(0.18)	5
SN 2005gn	IIn	55065	1479	−20.08(0.42)	−20.65(0.38)	14
SN 2005ip	*IIn*	*54627*	*948*	*−20.70(0.52)*	*−21.42(0.52)*	*17*
		55736	*2057*	*−19.88(0.52)*	*−20.75(0.52)*	*15*
		56475[b]	*2796*	*−19.17(0.52)*	*−20.02(0.52)*	*This work*
		56844[c]	*3165*	*−18.93(0.52)*	*−19.74(0.52)*	*This work*
		57228[d]	*3549*	*−18.73(0.52)*	*−19.47(0.52)*	*This work*
SN 2006E	Ia	53955	208	−13.13(0.35)	−12.99(0.45)	This work
SN 2006X	Ia	53922	152	−15.27(0.45)	−14.13(0.54)	18
SN 2006bc	II-P	54356	537	−13.55(0.78)	−14.13(0.73)	19
SN 2006bp	*II-P*	*54235*	*401*	*−15.60(0.44)*	*−16.20(0.45)*	*8*
		54462	*628*	*−15.40(0.44)*	*−15.65(0.45)*	*8*
		54600	*767*	*−15.36(0.45)*	*−15.69(0.45)*	*8*
		55195	*1361*	*−15.35(0.45)*	*−15.54(0.47)*	*8*
SN 2006ce	Ia	53955	90	−15.29(0.40)	−14.32(0.47)	This work
SN 2006jc	Ibn	54227	210	−17.46(0.48)	−18.23(0.47)	20
		54429	412	−15.20(0.53)	−16.23(0.50)	20
SN 2006jd	*IIn*	*55169*	*1149*	*−21.40(0.14)*	*−22.17(0.14)*	*17*
		55734	*1714*	*−20.68(0.14)*	*−21.62(0.14)*	*21*
		56453[b]	*2433*	*−19.68(0.17)*	*−20.74(0.15)*	*This work*
		56820[c]	*2800*	*−19.30(0.18)*	*−20.31(0.16)*	*This work*
SN 2006mq	Ia	54226	196	−13.71(0.29)	−11.94(0.79)	1
SN 2006my	II-P	54149	205	−17.18(0.59)	−17.49(0.59)	8
		54285	342	−16.95(0.94)	−17.02(0.58)	8
		54503	559	−16.87(0.59)	−16.91(0.59)	8
SN 2006ov	II-P	54285	321	−15.43(0.55)	−15.98(0.54)	8
		54503	539	−15.36(0.55)	−15.84(0.54)	8
SN 2006qq	*IIn*	*55117*	*1048*	*−19.88(0.13)*	*−20.70(0.11)*	*14*
		55874	*1805*	*−19.07(0.23)*	*−20.07(0.15)*	*15*
		56403[b]	*2334*	*−18.95(0.23)*	*−19.50(0.22)*	*This work*
SN 2007af	Ia	54324	164	−15.13(0.59)	−13.85(0.75)	18
SN 2007gr	Ic	54357	30	−18.00(0.96)	−18.22(0.96)	22
SN 2007it	II-P	54699	343	−15.20(0.30)	−16.67(0.28)	23
		54909	553	−16.04(0.28)	−16.65(0.28)	23
		55066	710	−15.05(0.30)	−16.07(0.29)	23
		55290	934	−13.13(0.50)	−15.00(0.32)	This work
		55441	1085	non	−14.50(0.35)	This work
		55663	1307	non	−14.18(0.38)	This work
SN 2007le	Ia	54464	78	−16.19(0.33)	−14.83(0.38)	18
SN 2007oc	II-P	54659	251	−16.91(0.40)	−17.94(0.40)	8
		54823	415	−16.35(0.40)	−16.88(0.40)	8
		55043	634	−15.57(0.42)	−14.55(0.48)	8
		55168	759	−15.81(0.42)	−15.33(0.44)	8

Table 6
(Continued)

Object	Type	MJD−2,450,000	Epoch (days)	Absolute mag. 3.6 μm	Absolute mag. 4.5 μm	Source of Data[a]
SN 2007od	II-P	54698	292	−16.13(0.31)	−16.99(0.29)	24
		54859	453	−14.98(0.39)	−16.02(0.33)	24
		55065	659	−14.48(0.43)	−14.48(0.51)	24
		55821	1415	−13.37(0.64)	−13.04(0.90)	This work
SN 2007rt	*IIn*	*55203*	*780*	*−21.74(0.19)*	*−22.43(0.18)*	*14*
		55733	*1304*	*−21.76(0.18)*	*−22.16(0.18)*	*15*
		56465[b]	*2042*	*−19.15(0.25)*	*−19.94(0.23)*	*This work*
SN 2007sq	II-P	54596	154	−17.41(0.82)	…	This work
SN 2007sr	Ia	54528	76	−16.43(0.44)	−15.08(0.50)	18
SN 2008J	IIn	55073	593	−21.25(0.17)	−21.88(0.16)	15
SN 2008Q	Ia	54727	236	−13.70(0.65)	−13.91(0.69)	25
SN 2008cg	*IIn*	*55065*	*474*	*−20.32(0.37)*	*−21.01(0.37)*	*14*
		55817	*1226*	*−16.70(0.70)*	*−18.33(0.58)*	*15*
SN 2008en	*IIn*	*55067*	*386*	*−20.73(0.13)*	*−21.38(0.13)*	*14*
		55812	*1131*	*−19.31(0.23)*	*−20.26(0.19)*	*15*
		56378[b]	*1697*	*−18.61(0.31)*	*−19.56(0.26)*	*This work*
SN 2008fq	II	55892	1168	−15.44(0.68)	−16.26(0.51)	This work
SN 2008gm	*IIn*	*55062*	*301*	*−17.55(0.23)*	*−17.76(0.24)*	*14*
		55796	*1035*	*−17.58(0.22)*	*−17.66(0.25)*	*15*
		56531[b]	*1770*	*−17.53(0.23)*	*−17.60(0.26)*	*This work*
SN 2008ip	*IIn*	*55088*	*438*	*−17.13(0.67)*	*−17.97(0.49)*	*14*
SN 2008jb	II	55076	287	−15.48(0.68)	−16.63(0.68)	26
		55113	324	−15.04(0.68)	−16.18(0.68)	26
SN 2009E	II-P	55381	547	−14.25(0.43)	−16.15(0.11)	This work
SN 2009H	*II*	*55077*	*243*	*−17.79(0.06)*	*−18.68(0.06)*	*This work*
		55116	*282*	*−17.54(0.07)*	*−18.53(0.06)*	*This work*
SN 2009af	*II*	*55077*	*199*	*−16.85(0.40)*	*−18.14(0.38)*	*This work*
		55107	*229*	*−16.34(0.40)*	*−17.76(0.38)*	*This work*
SN 2009at	*II*	*55375*	*474*	*16.01(0.42)*	*−16.56(0.42)*	*This work*
		55406	*505*	*−15.93(0.42)*	*−16.51(0.42)*	*This work*
SN 2009em	Ic	55073	117	−14.54(0.67)	−16.40(0.65)	This work
SN 2009gj	IIb	55070	68	−16.01(0.42)	−17.16(0.41)	This work
SN 2009ig	Ia	55076	13	−18.59(0.11)	−18.79(0.12)	18
		55115	52	−17.33(0.16)	−16.45(0.27)	18
SN 2009ip[e]	*IIn*	*56323*	*130*	*−15.72(0.26)*	*−16.40(0.25)*	*27*
		56498	*305*	*−14.08(0.39)*	*−15.02(0.34)*	*27*
		56518	*325*	*−14.05(0.40)*	*−14.95(0.35)*	*27*
		56531	*338*	*−13.94(0.41)*	*−14.88(0.36)*	*27*
		56905[c]	*712*	*−12.43(0.75)*	*−13.64 0.56)*	*This work*
		57278[d]	*1085*	*−12.03(0.90)*	*−13.32(0.64)*	*This work*
		57617[f]	*1424*	*−12.08(0.88)*	*−13.06(0.71)*	*This work*
SN 2009iu	*Ib*	*55142*	*67*	*−17.55(0.31)*	*−18.48(0.30)*	*This work*
SN 2009jf	Ib	55201	100	−16.86(0.46)	−17.92(0.46)	This work
SN 2009jr	Ia	55150	38	−17.45(0.18)	non	This work
		55161	49	−17.25(0.18)	non	This work
		55171	59	−16.52(0.18)	non	This work
SN 2009js	II-P p.	55117	2	−15.95(0.76)	−16.20(0.76)	28
SN 2009mk	IIb	55405	225	−15.09(0.20)	−15.94(0.20)	This work
SN 2010B	*Ia*	*55246*	*43*	*−17.16(0.24)*	*−16.68(0.32)*	*This work*
		55281	*78*	*−16.71(0.27)*	*−16.26(0.38)*	*This work*
		55311	*108*	*−16.52(0.29)*	*−16.19(0.39)*	*This work*
		55343	*140*	*−16.47(0.29)*	*−16.35(0.36)*	*This work*
SN 2010F	II	55416	207	−15.46(0.66)	−17.10(0.54)	This work
		55587	378	−13.93(1.51)	−15.40(0.74)	This work
		55740	531	non	−13.65(1.20)	This work
SN 2010jl	IIn	55570	67	−21.40(0.15)	−21.91(0.15)	29
		55732	229	−21.27(0.15)	−21.87(0.15)	30
		55943	440	−22.14(0.15)	−22.60(0.15)	30
		56099	596	−22.16(0.15)	−22.64(0.15)	30
		56322	819	−22.04(0.15)	−22.58(0.15)	30
		56472	969	−22.23(0.15)	−22.83(0.15)	This work
		56846	1343	−21.53(0.15)	−22.31(0.15)	This work
		57228[d]	1725	−20.76(0.15)	−21.75(0.15)	This work

Table 6
(Continued)

Object	Type	MJD−2,450,000	Epoch (days)	Absolute mag.		Source of Data[a]
				3.6 μm	4.5 μm	
SN 2010gp	Ia	55498	107	−16.60(0.38)	−16.62(0.49)	This work
SN 2010mc	*IIn*	*56814*	*1386*	*−18.78(0.33)*	*−19.32(0.33)*	*This work*
		57163	*1735*	*−18.68(0.35)*	*−19.22(0.34)*	*This work*
SN 2011A	IIn	55649	86	−16.04(0.39)	−16.32(0.36)	This work
SN 2011ae	Ia	55616	12	−18.62(0.05)	−18.71(0.06)	This work
SN 2011dh	IIb	55730	17	−17.71(0.11)	−18.10(0.10)	31
		55736	23	−17.90(0.11)	−18.27(0.11)	31
		55743	30	−17.89(0.11)	−18.27(0.11)	31
		55750	37	−17.86(0.11)	−18.28(0.11)	31
		55758	44	−17.76(0.11)	−18.27(0.11)	31
		55765	52	−17.60(0.11)	−18.23(0.11)	31
		55771	58	−17.44(0.11)	−18.19(0.11)	31
		55778	65	−17.26(0.11)	−18.14(0.11)	31
		55785	71	−17.07(0.11)	−18.07(0.11)	31
		55797	84	−16.72(0.11)	−17.94(0.11)	31
		55963	250	−15.18(0.11)	−16.19(0.11)	31
		55993	280	−15.01(0.11)	−16.47(0.11)	31
		56026	312	−13.98(0.12)	−15.27(0.11)	31
		56103	390	−12.43(0.28)	−14.00(0.14)	31
		56135	422	−12.12(0.37)	−13.55(0.18)	31
		56168	454	−11.88(0.45)	−13.29(0.21)	31
		56337	623	−10.95(1.04)	−12.01(0.61)	32
SN 2011dq	II	56955	1259	−18.20(0.28)	−18.41(0.27)	This work
SN 2011dx	Ia−pec.	55864	125	−15.02(0.55)	non	This work
SN 2011fe	Ia	55961	145	−14.87(0.17)	−13.73(0.18)	25
		55981	165	−14.55(0.18)	−13.44(0.18)	25
		56048	233	−13.61(0.18)	−13.02(0.19)	25
		56165	349	−11.77(0.24)	−11.75(0.30)	25
		56337	522	non	−11.16(0.50)	25
		56348	533	non	−11.27(0.39)	25
SN 2011fh	IIn	56383	586	−15.07(0.56)	−16.74(0.45)	This work
SN 2011ft	*Ib*	*56060*	*257*	*−18.68(0.21)*	…	*This work*
SN 2011ht	IIn	55833	638	non	−12.90(0.74)	This work
SN 2011ir	*IIn*	*55886*	*832*	*−16.98(0.48)*	*−17.78(0.44)*	*This work*
SN 2011iy	Ia	56932	1028	…	−12.79(0.36)	This work
SN 2011ja	II-P	56012	106	−16.22(0.28)	−16.99(0.28)	33
		56393	488	−16.25(0.28)	−17.07(0.28)	33
		56544	639	−15.48(0.28)	−16.47(0.28)	33
		56764	859	−14.37(0.30)	−15.70(0.29)	33
		56787	882	−14.21(0.31)	−15.56(0.29)	1
		56800	895	−14.13(0.32)	−15.44(0.29)	1
		56912	1007	−13.36(0.35)	−15.00(0.29)	1
		57136	1231	…	−14.39(0.29)	1
		57143	1238	…	−14.27(0.29)	1
		57164	1259	…	−14.04(0.29)	1
		57288	1382	non	−13.22(0.28)	1
PTF11kx	*Ia-CSM*	*56816*	*1237*	*−19.63(0.48)*	*−20.31(0.58)*	*34*
		57397	*1818*	*−18.64(1.11)*	*−19.56(1.11)*	*34*
PTF11qcj	Ic	56014	174	−17.53(0.61)	−18.31(0.48)	35
		56103	263	−16.42(0.84)	−17.34(0.57)	35
SN 2012aw	II-P	56360	358	−13.93(0.25)	−15.88(0.25)	This work
		56489	487	−12.80(0.33)	−14.70(0.26)	This work
SN 2012ca	*Ia-CSM*	*56446*	*404*	*−20.68(0.18)*	*−21.34(0.17*	*This work*
		56619	*577*	*−20.89(0.17)*	*−21.71(0.17)*	*This work*
		56820	*778*	*−19.69(0.19)*	*−21.02(0.18)*	*This work*
SN 2012cd	*IIb*	*56090*	*37*	*−18.56(0.19)*	*−19.07(0.19)*	*This work*
SN 2012cg	Ia	56140	58	−16.44(0.24)	−15.58(0.25)	18
		56153	71	−16.30(0.24)	−15.34(0.26)	18
		56163	81	−16.04(0.24)	−15.07(0.27)	18
		56175	93	−15.88(0.25)	−14.92(0.28)	18
SN 2012fh	Ic	56117	8	−17.64(0.44)	−17.92(0.44)	This work
		56122	13	−17.74(0.44)	−17.98(0.44)	This work
		56323	214	−16.40(0.44)	−17.52(0.44)	This work

Table 6
(Continued)

Object	Type	MJD−2,450,000	Epoch (days)	Absolute mag. 3.6 μm	Absolute mag. 4.5 μm	Source of Data[a]
		56356	247	−15.87(0.45)	−17.10(0.45)	This work
		56692	583	non	−12.39(0.95)	This work
SN 2013E	*Ia*	*56376*	*80*	*−16.17(0.57)*	⋯	*This work*
SN 2013L	*IIn*	*56944*	*630*	*−20.44(0.15)*	*−21.08(0.15)*	*36*
		57164	*850*	*−20.34(0.16)*	*−21.04(0.15)*	*36*
SN 2013ai	II	56671	319	−14.64(1.35)	⋯	1
		56790	448	⋯	−14.77(1.36)	1
		56816	474	non	−14.59(1.37)	1
		57057	705	−12.08(1.21)	−14.20(1.14)	1
SN 2013am	II	56715	343	−13.70(0.50)	−14.10(0.49)	1
		56741	369	−13.44(0.55)	−14.45(0.45)	1
		56865	493	−11.28(1.15)	−13.39(0.64)	1
SN 2013bu	II	56690	287	−14.86(0.47)	−15.90(0.42)	1
		56905	502	non	−14.22(0.41)	1
SN 2013cj	*IIn*	*56815*	*394*	*−22.04(0.17)*	*−22.42(0.17)*	*This work*
		57168	*747*	*−22.14(0.17)*	*−22.64(0.17)*	*This work*
SN 2013df	IIb	56715	268	−14.19(0.34)	−15.48(0.34)	1
		56742	294	−13.57(0.44)	−15.17(0.37)	1
		56871	423	−12.77(0.49)	−14.00(0.33)	1
		56906	459	−12.69(0.52)	−13.87(0.35)	1
		57272	824	−12.59(0.55)	−13.48(0.42)	1
SN 2013dk	Ic	56733	268	−16.05(0.40)	−16.79(0.40)	1
		56734	269	−15.89(0.40)	−16.80(0.40)	1
		56758	292	−15.62(0.41)	−16.48(0.40)	1
		56763	298	−15.71(0.41)	−16.42(0.41)	1
		56894	428	−14.85(0.41)	−15.51(0.42)	1
		57109	644	non	−13.83(0.44)	1
SN 2013dn	*Ia-CSM*	*56920*	*463*	*−20.70(0.24)*	*−21.46(0.24)*	*This work*
		57285	*828*	*−19.66(0.32)*	*−20.36(0.31)*	*This work*
SN 2013dy	Ia	56691	208	−13.42(0.72)	−12.25(0.75)	This work
		56731	248	−12.72(0.73)	−12.25(0.75)	This work
SN 2013ee	II	56677	191	−14.95(0.68)	−16.78(0.61)	This work
		56706	220	−15.33(0.63)	−16.71(0.62)	This work
		56827	341	−14.81(0.71)	−15.85(0.63)	This work
SN 2013ej	II-P/L	56735	238	−15.87(0.18)	−17.02(0.14)	37
		56758	261	−15.58(0.18)	−16.76(0.13)	37
		56937	439	−12.62(0.22)	−14.37(0.17)	37
		56965	468	−12.11(0.41)	−13.98(0.21)	37
		56970	473	−12.20(0.16)	−13.81(0.21)	37
		57321	823	non	−10.97(0.43)	37
		57334	837	non	−10.88(0.47)	37
		57475	978	non	−11.20(0.35)	37
		57482	985	non	−11.81(0.24)	37
		57504	1006	non	−11.89(0.21)	37
		57680[g]	1182	non	−11.58(0.58)	This work
		57695[h]	1197	non	−11.70(0.52)	This work
		57855[g]	1357	non	−11.32(0.45)	This work
SN 2013ff	Ic	56682	147	−16.46(0.40)	−17.89(0.31)	This work
SN 2014C	Ib	56707	45	−18.84(0.37)	−19.66(0.37)	1
		56905	243	−18.18(0.37)	−18.91(0.37)	1
		56937	274	−18.34(0.37)	−19.04(0.37)	1
		57284	622	−18.57(0.37)	−19.44(0.37)	1
		57290	628	−18.49(0.37)	−19.30(0.37)	1
		57304	642	−18.50(0.37)	−19.47(0.37)	1
		57435	772	−18.22(0.37)	−19.23(0.37)	1
		57442	780	−18.18(0.37)	−19.22(0.37)	1
		57464	801	−18.15(0.37)	−19.22(0.37)	1
SN 2014G	II-L	57232	561	−14.86(0.31)	−16.13(0.26)	This work
SN 2014J	Ia	56685	8	non	−18.61(0.13)	18
		56695	17	−18.00(0.13)	−17.90(0.13)	18
		56700	23	−17.58(0.13)	−17.10(0.13)	18
		56707	29	−17.27(0.13)	−16.68(0.13)	18
		56712	34	−17.15(0.13)	−16.48(0.13)	18

Table 6
(Continued)

Object	Type	MJD−2,450,000	Epoch (days)	Absolute mag. 3.6 μm	Absolute mag. 4.5 μm	Source of Data[a]
		56718	41	−17.00(0.13)	−16.32(0.13)	18
		56807	129	−15.56(0.14)	−14.40(0.16)	18
		56816	138	−15.40(0.14)	−14.25(0.17)	18
		56831	154	−15.03(0.14)	−13.99(0.19)	18
		56846	168	−14.82(0.15)	−13.67(0.23)	18
SN 2014L	Ic	56723	40	−17.50(0.28)	−18.05(0.27)	1
		56750	67	−17.02(0.28)	−17.93(0.28)	1
		56890	206	−15.53(0.28)	−16.68(0.28)	1
SN 2014bi	II-P	56847	38	−16.11(0.46)	−16.32(0.46)	1
		57072	264	−11.77(0.51)	−14.74(0.51)	1
		57076	268	−11.98(0.49)	−14.68(0.51)	1
		57080	272	−11.99(0.49)	−14.68(0.51)	1
		57102	293	−12.08(0.49)	−14.49(0.53)	1
		57253	445	−12.51(0.49)	−13.86(0.83)	1
		57484[g]	676	−10.95(1.18)	−12.47(0.62)	This work
SN 2014cx	II-P	56955	53	−18.19(0.27)	−18.36(0.28)	This work
SN 2014df	Ib	56929	118	−15.55(0.38)	non	1
SN 2014dt	Iax	57259	309	−14.46(0.92)	−15.01(0.88)	38
		57267	317	−14.53(0.92)	−15.13(0.88)	38
		57286	336	−14.93(0.88)	−15.38(0.87)	38

Notes.
[a] Fluxes, distances, epochs, and $E(B-V)$ values originate from our current work or are adopted from the papers listed here.
[b] Additional notes: sources of new data of previously known positive *Spitzer* targets (PID): 90174 (PI Fox).
[c] 10139 (PI Fox).
[d] 11053 (PI Fox).
[e] In the case of SN 2009ip, epochs are given with respect to the SN-like outburst observed in 2012. Data marked with italics denote cases where image subtraction cannot be applied.
[f] 12099 (PI Fraser).
[g] 13053 (PI Kasliwal).
[h] 11063 (PI Kasliwal).

References. (1) Tinyanont et al. (2016), (2) Van Dyk (2013), (3) Szczygiel et al. (2012), (4) Meikle et al. (2006), (5) Fox & Filippenko (2013), (6) Meikle et al. (2007), (7) Meikle et al. (2005), (8) Szalai & Vinkó (2013), (9) Szalai et al. (2011), (10) Meikle et al. (2011), (11) Kotak et al. (2009), (12) Fabbri et al. (2011), (13) Kankare et al. (2014), (14) Fox et al. (2011), (15) Fox et al. (2013), (16) Gerardy et al. (2007), (17) Fox et al. (2010), (18) Johansson et al. (2017), (19) Gallagher et al. (2012), (20) Mattila et al. (2008), (21) Stritzinger et al. (2012), (22) Kochanek et al. (2011), (23) Andrews et al. (2011b), (24) Andrews et al. (2010), (25) McClelland et al. (2013), (26) Prieto et al. (2012), (27) Fraser et al. (2015), (28) Gandhi et al. (2013), (29) Andrews et al. (2011a), (30) Fransson et al. (2014), (31) Helou et al. (2013), (32) Ergon et al. (2015), (33) Andrews et al. (2016), (34) Graham et al. (2017), (35) Corsi et al. (2014), (36) Andrews et al. (2017), (37) Mauerhan et al. (2017), (38) Fox et al. (2016).
(This table is available in machine-readable form.)

Table 7
Dust Parameters of the Studied SNe (Pure Graphite Dust with a Grain Size of $a = 0.1$ μm)

Object	Type	Epoch (days)	R_{BB} (10^{16} cm)	v_{BB} (km s^{-1})	T_{dust} (K)	M_{dust} (10^{-5} $M_{\odot}$)	L_{dust} (10^6 $L_{\odot}$)	Notes
SN 1995N	*IIn*	*5067*	*2.4*	*550*	*350*	*<478*	*<3.8*	*Possible Si dust ($M = 1.4 \times 10^{-3}$ $M_{\odot}$, $T = 410$ K)*
SN 2001em	*Ib/c*	*1135*	*15.4*	*15,700*	*280*	*<22800*	*<58.4*	*+ hot comp. ($R = 10^{16}$ cm, $T = 1400$ K)*
SN 2001gd	IIb	952	0.06	80	730	0.21	0.1	
SN 2002bu	IIn	759	0.4	640	520	10.8	0.7	
SN 2002ic	Ia-CSM	795	8.5	12,370	590	1200	160	
		1179	8.8	8640	495	1600	87.0	
		1370	8.0	6760	480	1400	63.0	
SN 2003gd	II-P	409	0.4	1020	520	1.1	0.1	
SN 2003lo	IIn	256	0.6	2490	640	14.1	2.9	
		384	0.3	840	690	4.0	1.2	
SN 2004A	II-P	247	3.4	15,930	240	2438	2.9	+ hot comp. ($R = 0.05 \times 10^{16}$ cm, $T = 4800$ K)
		445	3.8	9885	270	852	1.8	
		563	2.2	4520	300	386	1.4	
SN 20004dj	II-P	267	0.2	870	890	0.3	0.4	+ cold comp. ($R = 1.5 \times 10^{16}$ cm, $T = 186$ K)
		850	0.4	540	630	1.1	0.3	+ cold comp. ($R = 4.3 \times 10^{16}$ cm, $T = 120$ K)
		1006	0.4	460	550	1.3	0.2	+ cold comp. ($R = 4.6 \times 10^{16}$ cm, $T = 110$ K)
		1237	0.4	370	490	1.4	0.1	+ cold comp. ($R = 6.5 \times 10^{16}$ cm, $T = 103$ K)
SN 2004et	II-P	300	0.4	1600	550	10.0	0.9	+ Possible Si dust ($M = 3.8 \times 10^{-5}$ $M_{\odot}$, $T = 900$ K)
		360	0.4	1300	520	11.0	0.7	+ Possible Si dust ($M = 5.6 \times 10^{-5}$ $M_{\odot}$, $T = 730$ K)
		465	0.4	1100	480	8.2	0.3	+ Possible Si dust ($M = 6.6 \times 10^{-5}$ $M_{\odot}$, $T = 650$ K)
		736	0.5	830	340	18.0	0.1	+ cold comp. ($R = 5.4 \times 10^{16}$ cm, $T = 110$ K)
		1125	0.4	1250	420	10.0	0.2	+ hot comp. ($R = 0.01 \times 10^{16}$ cm, $T = 6300$ K)
		1222	0.5	650	420	11.0	0.2	+ cold comp. ($R = 4.5 \times 10^{16}$ cm, $T = 120$ K)
SN 2005ad	II-P	198	0.3	1755	630	6.0	1.1	
		364	0.2	635	580	3.8	0.4	
SN 2005af	II-P	194	0.8	4770	510	43.6	2.5	
		399	0.4	1160	510	10.9	0.6	*Possible Si dust ($M = 1.6 \times 10^{-5}$ $M_{\odot}$, $T = 640$ K)*
		576	0.6	1205	340	64.5	0.4	*Possible Si dust ($M = 2.6 \times 10^{-5}$ $M_{\odot}$, $T = 460$ K)*
		772	0.8	1200	290	58.8	0.2	*Possible Si dust ($M = 0.7 \times 10^{-5}$ $M_{\odot}$, $T = 430$ K)*
SN 2005at	Ic	569	2.7	5490	270	<640.0	<1.4	+ hot comp. ($R = 7.0 \times 10^{13}$ cm, $T = 10\,500$ K)
SN 2005cp	*IIn*	*1523*	*3.6*	*2730*	*550*	*<680*	*<56.0*	
		2254	*2.0*	*1040*	*730*	*<52.0*	*<22.0*	*Only a two-point mid-IR SED*
SN 2005gj	Ia-CSM	139	3.3	27,480	845	100	100	
		365	4.0	12,680	845	200	150	
		510	6.8	15,430	725	600	230	
SN 2005gn	IIn	1479	1.5	1180	740	190	84.0	Only a two-point mid-IR SED
SN 2005ip	*IIn*	*948*	*4.8*	*5860*	*470*	*<4200*	*<140*	
		2057	*8.5*	*4790*	*510*	*<1900*	*<100*	*Only a two-point mid-IR SED*
SN 2006bp	*II-P*	*401*	*4.5*	*12,990*	*370*	*<480*	*<4.7*	*+ cold comp. ($R = 24 \times 10^{16}$ cm, $T = 110$ K)*
		628	*5.5*	*10,140*	*330*	*<1000*	*<4.4*	
		767	*5.1*	*7695*	*350*	*<690*	*<4.6*	*+ cold comp. ($R = 42 \times 10^{16}$ cm, $T = 80$ K)*
SN 2006jc	Ibn	210	1.3	7160	600	59.5	8.6	
		412	1.5	4210	440	71.6	1.9	
SN 2006jd	*IIn*	*1149*	*6.3*	*6380*	*580*	*<3000*	*<320*	*Only a two-point mid-IR SED*
		1714	*11.4*	*7670*	*530*	*<4000*	*<230*	*Only a two-point mid-IR SED*
SN 2006my	II-P	205	3.8	21,455	280	4920	12.6	+ hot comp. ($R = 0.1 \times 10^{16}$ cm, $T = 3700$ K)
		342	3.7	12,520	300	3074	11.1	+ cold comp. ($R = 33.5 \times 10^{16}$ cm, $T = 120$ K)
		559	4.2	8695	290	3960	12.1	+ cold comp. ($R = 76 \times 10^{16}$ cm, $T = 90$ K)
SN 2006ov	II-P	321	5.1	18,390	280	2500	6.4	
		539	3.4	7300	310	976	4.1	
SN 2006qq	*IIn*	*1048*	*4.5*	*5010*	*500*	*<1600*	*<77.0*	*Only a two-point mid-IR SED*
		1805	*3.3*	*2120*	*770*	*<130*	*<75.0*	*Only a two-point mid-IR SED*
SN 2007it	II-P	343	0.3	910	640	5.0	1.0	
		553	0.4	900	640	10.6	2.0	
		710	0.6	960	530	15.9	1.1	
		934	1.8	2180	350	133	1.0	
SN 2007oc	II-P	251	5.7	26,285	340	310	9.8	
		415	4.9	13,665	340	370	6.1	
SN 2007rt	*IIn*	*780*	*5.4*	*8000*	*625*	*<2200*	*<370*	*Only a two-point mid-IR SED*
		1304	*8.5*	*7560*	*555*	*<2300*	*<190*	*Only a two-point mid-IR SED*
SN 2008J	IIn	593	3.3	6460	700	870	290	Only a two-point mid-IR SED
SN 2008cg	*IIn*	*474*	*3.4*	*8320*	*600*	*<1300*	*<180*	*Only a two-point mid-IR SED*
		1226	*3.0*	*2860*	*575*	*<310*	*<32.0*	*Only a two-point mid-IR SED*

Table 7
(Continued)

Object	Type	Epoch (days)	R_{BB} (10^{16} cm)	v_{BB} (km s^{-1})	T_{dust} (K)	M_{dust} (10^{-5} $M_{\odot}$)	L_{dust} (10^{6} $L_{\odot}$)	Notes
SN 2008en	*IIn*	*386*	*2.9*	*8790*	*680*	*<670*	*<180*	*Only a two-point mid-IR SED*
		1131	*5.7*	*5810*	*560*	*<680*	*<62.0*	*Only a two-point mid-IR SED*
SN 2008fq	II	1168	0.4	420	600	9.5	1.3	Only a two-point mid-IR SED
SN 2008gm	*IIn*	*301*	*0.4*	*1460*	*720*	*<6.5*	*<2.5*	*Only a two-point mid-IR SED*
		1035	*0.5*	*530*	*1070*	*<1.6*	*<6.4*	*Only a two-point mid-IR SED*
SN 2008ip	*IIn*	*438*	*0.8*	*2000*	*610*	*<42.0*	*<5.9*	*Only a two-point mid-IR SED*
SN 2009E	II-P	547	3.0	6330	340	5080	3.5	Only a two-point mid-IR SED
SN 2009H	*II*	*243*	*1.6*	*7670*	*600*	*<93.2*	*<13.2*	*Only a two-point mid-IR SED*
		282	*1.8*	*7350*	*580*	*<95.3*	*<11.2*	*Only a two-point mid-IR SED*
SN 2009af	*II*	*199*	*2.4*	*14,130*	*460*	*<255*	*<8.5*	*Only a two-point mid-IR SED*
		229	*2.5*	*12,790*	*430*	*<295*	*<6.8*	*Only a two-point mid-IR SED*
SN 2009at	*II*	*474*	*0.3*	*780*	*750*	*<5.1*	*<2.5*	*Only a two-point mid-IR SED*
		505	*0.3*	*760*	*730*	*<5.5*	*<2.3*	*Only a two-point mid-IR SED*
SN 2009ip	*IIn*	*712*	*0.3*	*420*	*470*	*<3.8*	*<0.1*	*Only a two-point mid-IR SED*
		1085	*0.3*	*290*	*450*	*<3.8*	*<0.1*	*Only a two-point mid-IR SED*
		1424	*0.1*	*110*	*540*	*<0.9*	*<0.1*	*Only a two-point mid-IR SED*
SN 2009jf	Ib	100	1.5	17,360	520	*<98.5*	*<6.4*	2 mid-IR point + hot comp. ($R = 0.09 \times 10^{16}$ cm, $T = 5760$ K)
SN 2009mk	IIb	225	0.3	1290	860	3.5	3.8	Only a two-point mid-IR SED
SN 2010F	II	207	3.0	16,770	380	452.9	5.5	Only a two-point mid-IR SED
		378	1.0	3060	420	41.7	0.9	Only a two-point mid-IR SED
SN 2010jl	IIn	67	3.1	53,550	780	490	306	Only a two-point mid-IR SED
		229	3.7	18,700	720	668	265	Only a two-point mid-IR SED
		440	3.8	10,000	810	805	621	Only a two-point mid-IR SED
		596	4.1	7960	800	872	629	Only a two-point mid-IR SED
		819	4.6	6500	750	1090	544	Only a two-point mid-IR SED
		969	5.7	6810	720	1620	641	Only a two-point mid-IR SED
		1343	6.6	5690	620	2094	356	Only a two-point mid-IR SED
		1725	7.5	5030	540	2674	211	Only a two-point mid-IR SED
SN 2010mc	*IIn*	*1386*	*1.0*	*840*	*760*	*<50.4*	*<27.1*	*Only a two-point mid-IR SED*
		1735	*1.0*	*650*	*750*	*<49.0*	*<24.4*	*Only a two-point mid-IR SED*
SN 2011dh	IIb	250	0.7	3240	520	10.0	0.8	Only a two-point mid-IR SED
		280	1.6	6610	410	90.0	1.3	Only a two-point mid-IR SED
		312	0.7	2600	450	20.0	0.4	Only a two-point mid-IR SED
		390	0.6	1780	390	10.0	0.2	Only a two-point mid-IR SED
		422	0.4	1100	420	5.0	0.01	Only a two-point mid-IR SED
		454	0.3	870	420	4.0	0.01	Only a two-point mid-IR SED
		623	0.1	190	510	0.3	0.002	Only a two-point mid-IR SED
SN 2011dq	II	1259	0.3	260	1080	6.0	25.0	Only a two-point mid-IR SED
SN 2011fh	IIn	586	1.7	3280	360	439	4.0	Only a two-point mid-IR SED
SN 2011ir	*IIn*	*832*	*0.9*	*1180*	*610*	*<35.1*	*<5.4*	*Only a two-point mid-IR SED*
SN 2011ja	II-P	106	1.0	10,920	610	18.0	2.6	Only a two-point mid-IR SED
		488	1.1	2610	590	23.0	2.7	Only a two-point mid-IR SED
		639	1.1	1990	530	26.0	1.6	Only a two-point mid-IR SED
		859	1.2	1620	440	45.0	1.0	Only a two-point mid-IR SED
		881	1.2	1580	430	43.0	0.9	Only a two-point mid-IR SED
		1007	1.4	1610	380	76.0	0.7	Only a two-point mid-IR SED
PTF11kx	*Ia-CSM*	*1237*	*5.0*	*4680*	*590*	*<400*	*<57.0*	*Only a two-point mid-IR SED*
		1818	*5.0*	*3180*	*580*	*<200*	*<26.0*	*Only a two-point mid-IR SED*
PTF11qcj	Ic	174	1.0	6650	620	52.4	8.9	Only a two-point mid-IR SED
		263	0.9	3960	560	37.5	3.6	Only a two-point mid-IR SED
SN 2012ca	*Ia-CSM*	*404*	*3.3*	*9450*	*680*	*<537*	*<154*	*Only a two-point mid-IR SED*
		577	*5.3*	*10,630*	*610*	*<1302*	*<202*	*Only a two-point mid-IR SED*
		778	*10.4*	*15,470*	*450*	*<4445*	*<131*	*Only a two-point mid-IR SED*
SN 2012fh	Ic	214	1.4	7460	500	87.5	4.5	Only a two-point mid-IR SED
		247	1.4	6560	470	89.0	3.3	
SN 2013L	*IIn*	*630*	*2.6*	*4780*	*720*	*<341*	*<124*	*Only a two-point mid-IR SED*
		850	*3.4*	*4630*	*650*	*<573*	*<127*	*Only a two-point mid-IR SED*
SN 2013ai	II	705	0.6	820	400	13.0	0.2	Only a two-point mid-IR SED
SN 2013am	II	343	0.4	1490	630	3.1	0.6	Only a two-point mid-IR SED
		369	0.9	2760	480	21.0	0.8	Only a two-point mid-IR SED
		493	0.5	1130	510	5.6	0.3	Only a two-point mid-IR SED
SN 2013bu	II	287	0.7	2700	550	11.0	0.9	Only a two-point mid-IR SED

Table 7
(Continued)

Object	Type	Epoch (days)	R_{BB} (10^{16} cm)	v_{BB} (km s^{-1})	T_{dust} (K)	M_{dust} (10^{-5} $M_{\odot}$)	L_{dust} (10^{6} $L_{\odot}$)	Notes
SN 2013cj	*IIn*	*394*	*2.9*	*8550*	*880*	*<490*	*<614*	*Only a two-point mid-IR SED*
		747	*4.2*	*6570*	*780*	*<967*	*<606*	*Only a two-point mid-IR SED*
SN 2013df	IIb	268	1.0	4320	480	28.0	1.0	Only a two-point mid-IR SED
		294	1.0	3940	450	32.0	0.8	Only a two-point mid-IR SED
		423	1.3	3560	340	78.0	0.4	Only a two-point mid-IR SED
		459	0.3	760	520	2.6	0.1	Only a two-point mid-IR SED
		824	0.1	140	740	0.1	0.06	Only a two-point mid-IR SED
SN 2013dk	Ic	268	0.8	3450	620	12.0	1.9	Only a two-point mid-IR SED
		269	1.0	4320	560	21.0	1.9	Only a two-point mid-IR SED
		292	0.8	3170	570	14.0	1.4	Only a two-point mid-IR SED
		298	0.7	2720	640	7.4	1.4	Only a two-point mid-IR SED
		428	0.4	1080	660	2.6	0.6	Only a two-point mid-IR SED
SN 2013dn	*Ia-CSM*	*463*	*3.7*	*9250*	*670*	*<645*	*<170*	*Only a two-point mid-IR SED*
		828	*2.3*	*3215*	*660*	*<253*	*<61.0*	*Only a two-point mid-IR SED*
SN 2013ee	II	191	3.6	22,050	350	690	5.4	Only a two-point mid-IR SED
		220	1.6	8470	430	118	2.7	Only a two-point mid-IR SED
		341	0.6	1870	520	14.8	1.0	Only a two-point mid-IR SED
SN 2013ej	II-P/L	238	1.7	8300	490	62.0	2.9	Only a two-point mid-IR SED
		261	1.6	7100	465	72.0	2.2	Only a two-point mid-IR SED
		439	1.2	3160	360	64.0	0.4	Only a two-point mid-IR SED
SN 2013ff	Ic	147	2.9	22,830	420	419	8.6	Only a two-point mid-IR SED
SN 2014C	Ib	243	2.1	10,000	620	75.0	13.0	Only a two-point mid-IR SED
		274	2.2	9290	640	74.0	14.0	Only a two-point mid-IR SED
		622	3.2	5950	570	200	20.0	Only a two-point mid-IR SED
		628	2.8	5160	590	150	18.0	Only a two-point mid-IR SED
		642	3.7	6670	540	290	20.0	Only a two-point mid-IR SED
		772	3.6	5400	520	290	17.0	Only a two-point mid-IR SED
		780	3.6	5340	510	320	17.0	Only a two-point mid-IR SED
		801	3.8	5490	500	360	17.0	Only a two-point mid-IR SED
SN 2014G	II-L	561	1.0	2040	460	42.4	1.4	Only a two-point mid-IR SED
SN 2014L	Ic	206	1.6	8990	480	64.0	2.4	Only a two-point mid-IR SED
SN 2014bi	II-P	264	8.9	39,020	240	7200	4.9	Only a two-point mid-IR SED
		268	5.6	24,180	260	2500	2.7	Only a two-point mid-IR SED
		272	5.5	23,400	260	2600	2.6	Only a two-point mid-IR SED
		293	3.3	13,040	285	730	1.3	Only a two-point mid-IR SED
		445	0.5	1300	430	8.3	0.2	Only a two-point mid-IR SED
SN 2014dt	Iax	309	0.3	1120	710	1.3	0.5	Only a two-point mid-IR SED
		317	0.3	1100	680	1.8	0.5	Only a two-point mid-IR SED
		336	0.3	1030	770	1.3	0.8	Only a two-point mid-IR SED

Appendix B
Comparison of Single-epoch *Spitzer* Detections with Pre-explosion 2MASS *JHK* Data

Here, we present all the pairs of images *Spitzer*/IRAC + pre-explosion 2MASS K_s) and SED fittings (Figures 18 and 19, respectively), leading us to select the single-epoch positive detections, together with an example for negative detections (Figure 20).

The basic astrometric criterion of a potential positive detection was an agreement between the absolute SN coordinates and the position of the photometric center of the mid-IR point source within two IRAC pixels (1$''$.2). Corresponding angular distances, and uncertainties of the absolute coordinates, together with pre-explosion 2MASS JHK_s magnitudes of positively detected SNe based on single-epoch *Spitzer*/IRAC imaging are shown in Table 8.

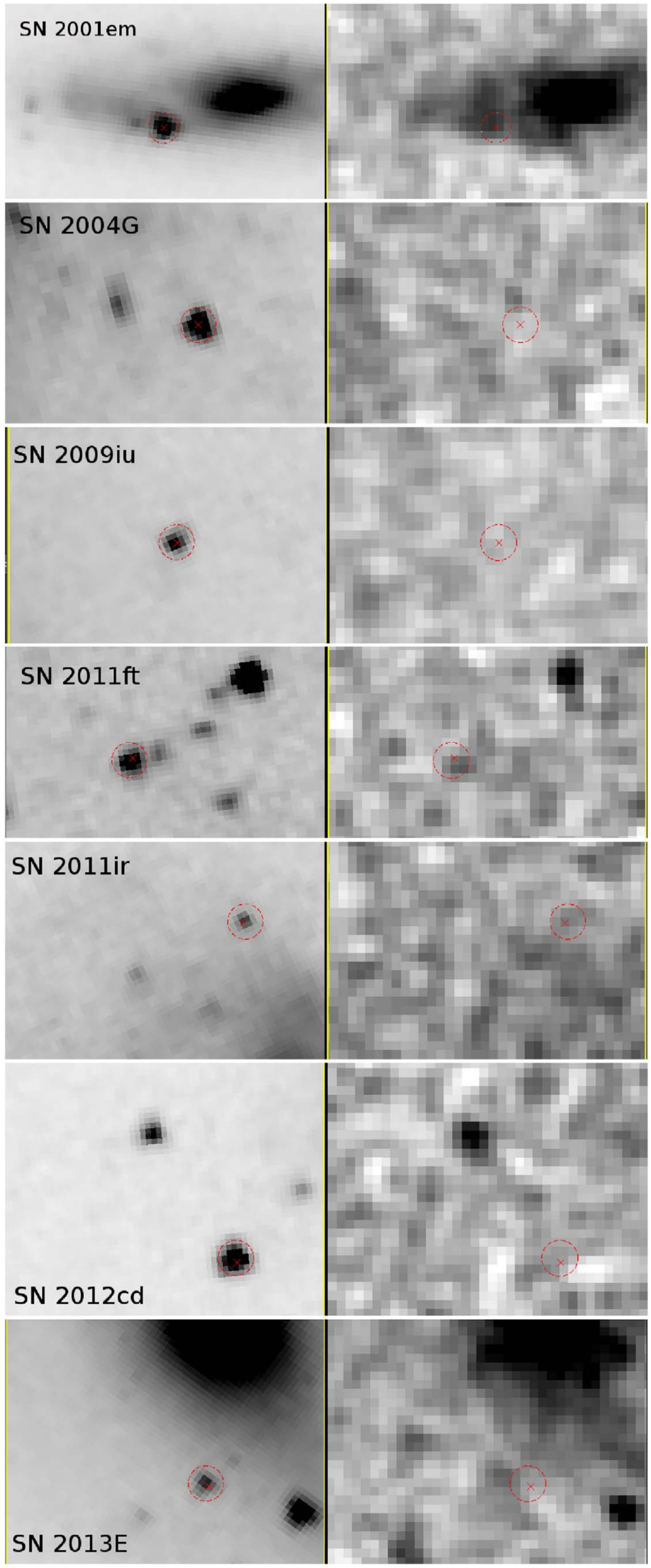

Figure 18. Comparison of single-epoch *Spitzer*/IRAC 3.6 micron images (left) of SNe (classified as positive detections) with pre-explosion 2MASS K_s images (right). Colors are inverted for better visibility. Red crosses denote the SN coordinates adopted from sources given in the Open Supernova Catalog, while red circles with radii of 2″ show the typical PSF FWHM of point sources on IRAC images centered on the photometric centers of the mid-IR points sources.

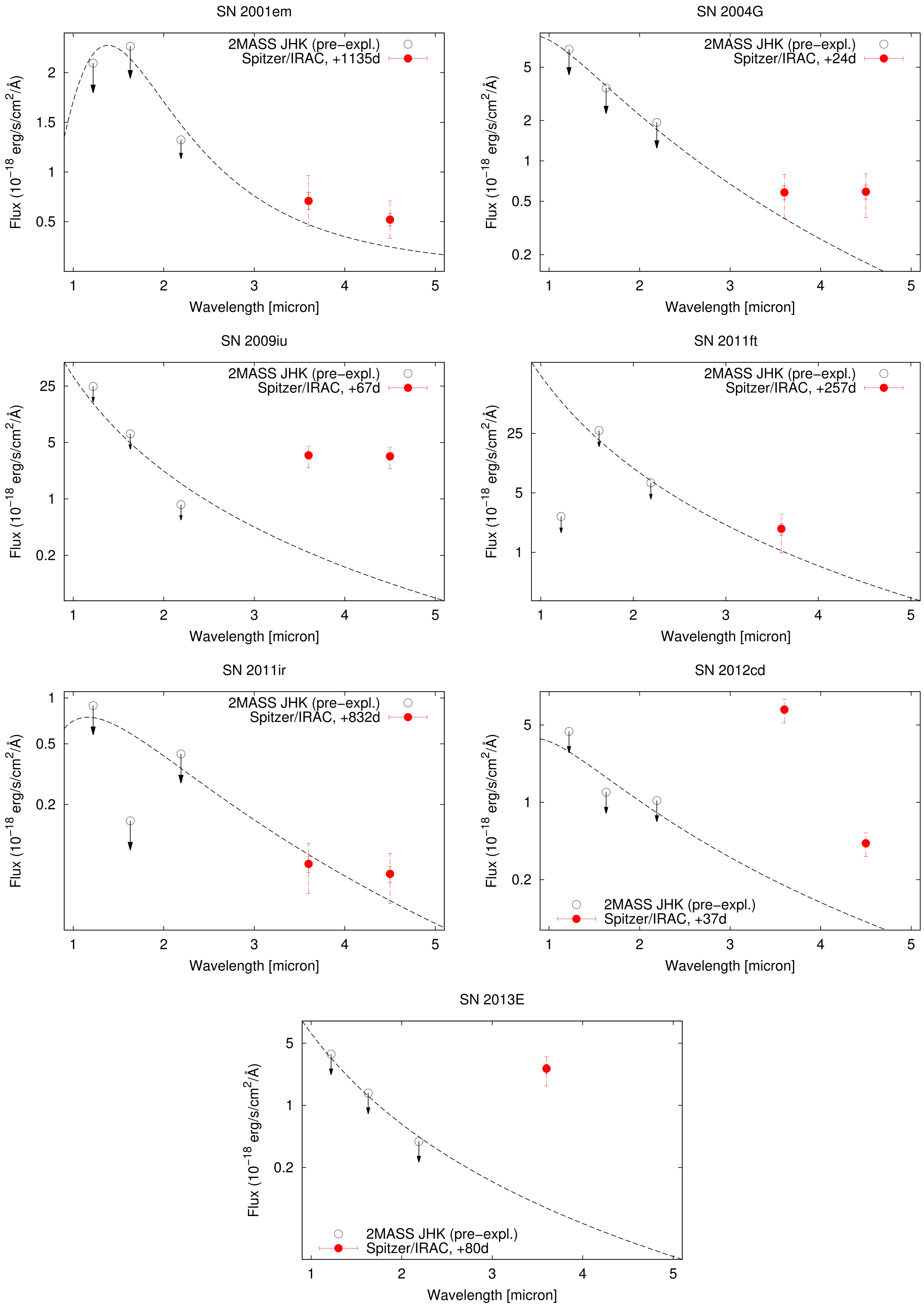

Figure 19. Comparison of pre-explosion 2MASS JHK_s (black open circles) and post-explosion mid-IR fluxes (red filled circles) in the cases of single-epoch *Spitzer*/IRAC SN observations classified as positive detections. Simple blackbodies are fitted to upper limits of JHK_s fluxes in order to see whether or not there can be any "real" mid-IR excess at post-explosion *Spitzer* images (see the text for details). In the cases of IRAC fluxes, the solid and dashed error bars denote 1σ and 3σ photometric errors, respectively.

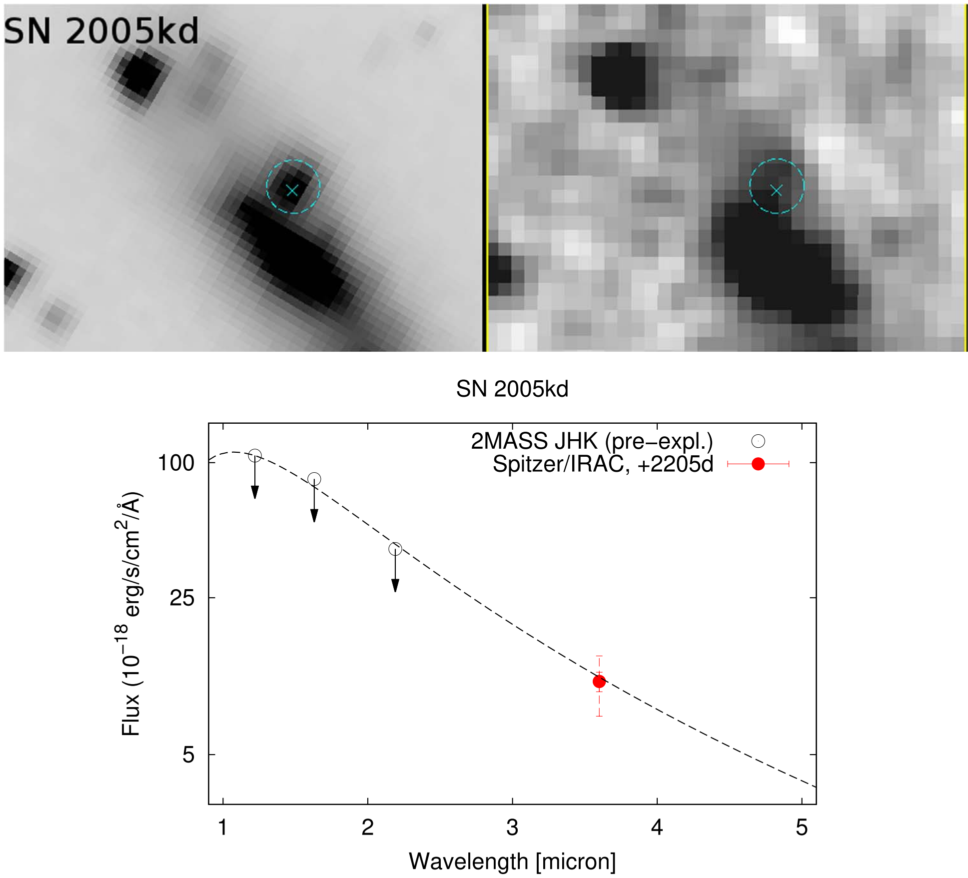

Figure 20. SN 2005kd: an example of single-epoch *Spitzer*/IRAC supernova observations classified as negative detections. Although one can see a mid-IR source at the position of the SN, some flux can be also detected on the pre-explosion 2MASS K_s image. Doing the final step of checking, no significant excess could be revealed at the 3.6 μm channel (the field was not observed in any other IRAC channels).

Table 8

Uncertainties of Absolute Coordinates (σR.A., σdecl.), Agreement of These Coordinates and Those of the Photometric Centers of Mid-IR Point Sources (ΔXY), and Pre-explosion 2MASS JHK_s Magnitudes (Estimating a General ±0.4 mag Error) of Positively Detected SNe Based on Single-epoch *Spitzer*/IRAC Imaging

Object	σR.A.	σDecl.	References	ΔXY	J (pre-exp.)	H (pre-exp.)	K_s (pre-exp.)
SN 2001em	<0."001	<0."001	1	<0."6	18.38(0.40)	17.16(0.40)	16.58(0.40)
SN 2004G	unknown	unknown	⋯	<0."6	17.05(0.40)	16.66(0.40)	16.15(0.40)
SN 2009iu	<0."1	<0."1	2	<0."6	18.15(0.40)	18.50(0.40)	19.54(0.40)
SN 2011ft	unknown	unknown	⋯	<1."2	20.60(0.40)	16.95(0.40)	17.33(0.40)
SN 2011ir	unknown	unknown	⋯	<1."2	19.25(0.40)	20.03(0.40)	17.78(0.40)
SN 2012cd	unknown	unknown	⋯	<1."2	20.03(0.40)	20.29(0.40)	19.33(0.40)
SN 2013E	unknown	unknown	⋯	<1."2	20.06(0.40)	20.03(0.40)	20.23(0.40)

Note. References: (1) Bietenholz & Bartel (2005), (2) Maza et al. (2009).

ORCID iDs

Tamás Szalai https://orcid.org/0000-0003-4610-1117
Ori D. Fox https://orcid.org/0000-0003-2238-1572
Ondřej Pejcha https://orcid.org/0000-0003-2512-2170
Tomás Müller https://orcid.org/0000-0003-3939-7167

References

Aldering, G., Bailey, S., Bongard, S., et al. 2006, CBET, 366, 1
Andrews, J. E., Clayton, G. C., Wesson, R., et al. 2011a, AJ, 142, 45
Andrews, J. E., Gallagher, J. S., Clayton, G. C., et al. 2010, ApJ, 715, 541
Andrews, J. E., Krafton, K. M., Clayton, G. C., et al. 2016, MNRAS, 457, 3241
Andrews, J. E., Smith, N., Fong, W.-F., & Milne, P. 2015, ATel, 7084, 1
Andrews, J. E., Smith, N., McCully, C., et al. 2017, MNRAS, 471, 4047
Andrews, J. E., Sugerman, B. E. K., Clayton, G. C., et al. 2011b, ApJ, 731, 47
Arbour, R., & Briggs, D. 2009, CBET, 1964, 1
Balanutsa, P., Parhomenko, A. V., Tlatov, A., et al. 2011, ATel, 3610, 1
Benetti, S., Valenti, S., Magazzu, A., & Harutyunyan, A. 2009, CBET, 1667, 1
Bietenholz, M. F., & Bartel, N. 2005, ApJL, 625, L99
Blackman, J., Schmidt, B., & Kerzendorf, W. 2006, CBET, 541, 1
Bode, M. F., & Evans, A. 1980, MNRAS, 193, 21
Boles, T. 2009, CBET, 1648, 1
Boles, T. 2011, CBET, 2851, 1
Bose, S., Sutaria, F., Kumar, B., et al. 2015, ApJ, 806, 160
Brimacombe, J., Zaggia, S., Barbieri, M., et al. 2013, CBET, 3647, 1
Burket, J., & Li, W. 2005, IAUC, 8472, 1
Casper, C., Zheng, W., Li, W., Filippenko, A. V., & Cenko, S. B. 2013, CBET, 3588, 1
Chakraborti, S., Ray, A., Smith, R., et al. 2016, ApJ, 817, 22
Chen, J., Wang, X.-F., Wang, X.-L., et al. 2011, CBET, 2943, 2

Chevalier, R. A., & Soderberg, A. M. 2010, ApJL, 711, L40
Chomiuk, L., Soderberg, A. M., Chevalier, R. A., et al. 2016, ApJ, 821, 119
Chornock, R., & Berger, E. 2009, CBET, 2086, 1
Chugai, N. N., & Chevalier, R. A. 2006, ApJ, 641, 1051
Ciroi, S., di Mille, F., Carco, M., et al. 2009, CBET, 1697, 2
Corsi, A., Ofek, E. O., Gal-Yam, A., et al. 2014, ApJ, 782, 42
Cortini, G. 2009, CBET, 1697, 1
Cortini, G., Brimacombe, J., Tomasella, L., et al. 2013, CBET, 3597, 1
Dall'Ora, M., Botticella, M. T., Pumo, M. L., et al. 2014, ApJ, 787, 139
de Jaeger, T., Anderson, J. P., Pignata, G., et al. 2015, ApJ, 807, 63
Dhungana, G., Kehoe, R., Vinkó, J., et al. 2016, ApJ, 822, 6
Drake, A. J., Djorgovski, S. G., Graham, M. J., et al. 2013, CBET, 3570, 1
Drescher, C., Parker, S., & Brimacombe, J. 2012, CBET, 3101, 1
Dwek, E. 1983, ApJ, 274, 175
Dwek, E., Arendt, R. G., Bouchet, P., et al. 2010, ApJ, 722, 425
Elias-Rosa, N., Navasardyan, H., Harutunyan, A., et al. 2005, IAUC, 8479, 3
Ercolano, B., Barlow, M. J., & Sugerman, B. E. K. 2007, MNRAS, 375, 753
Ergon, M., Jerkstrand, A., Sollerman, J., et al. 2015, A&A, 580, 142
Fabbri, J., Otsuka, M., Barlow, M. J., et al. 2011, MNRAS, 418, 1285
Filippenko, A. V., Matheson, T., & Ho, L. C. 1993, ApJL, 415, L103
Fitzpatrick, E. L., & Massa, D. 2007, ApJ, 663, 320
Folatelli, G., Gutierrez, C., & Pignata, G. 2010, CBET, 2390, 1
Foley, R. J. 2009, CBET, 1858, 1
Foley, R. J. 2010, CBET, 2137, 1
Foley, R. J., Jha, S. W., Pan, Y-C., et al. 2016, MNRAS, 461, 433
Fox, O. D., Chevalier, R. A., Dwek, E., et al. 2010, ApJ, 725, 1768
Fox, O. D., Chevalier, R. A., Skrutskie, M. F., et al. 2011, ApJ, 741, 7
Fox, O. D., & Filippenko, A. V. 2013, ApJL, 772, L6
Fox, O. D., Filippenko, A. V., Skrutskie, M. F., et al. 2013, AJ, 146, 2
Fox, O. D., Johansson, J., Kasliwal, M., et al. 2016, ApJL, 816, L13
Fox, O. D., Silverman, J. M., Filippenko, A. V., et al. 2015, MNRAS, 447, 772
Fransson, C., Ergon, M., Challis, P., et al. 2014, ApJ, 797, 118
Fraser, M., Inserra, C., Jerkstrand, A., et al. 2013, MNRAS, 433, 1332
Fraser, M., Kotak, R., Pastorello, A., et al. 2015, MNRAS, 453, 3886
Gall, C., Andersen, A. C., & Hjorth, J. 2011, A&A, 528, A13
Gall, C., Hjorth, J., Watson, D., et al. 2014, Natur, 511, 326
Gallagher, J. S., Sugerman, B. E. K., Clayton, G. C., et al. 2012, ApJ, 753, 109
Gandhi, P., Yamanaka, M., Tanaka, M., et al. 2013, ApJ, 767, 166
Gerardy, C. L., Fesen, R. A., Nomoto, K., et al. 2002, ApJ, 575, 1007
Gerardy, C. L., Meikle, W. P. S., Kotak, R., et al. 2007, ApJ, 661, 995
Graham, J., & Li, W. 2005, IAUC, 8459, 3
Graham, J. R., & Meikle, W. P. S. 1986, MNRAS, 221, 789
Graham, M. L., Harris, C. E., Fox, O. D., et al. 2017, ApJ, 843, 102
Guillochon, J., Parrent, J., Kelley, L. Z., & Margutti, R. 2017, ApJ, 835, 64
Harutyunyan, A., Bufano, F., & Benetti, S. 2009, CBET, 1722, 1
Helou, G., Kasliwal, M. M., Ofek, E. O., et al. 2013, ApJL, 778, L19
Holoien, T. W.-S., Brown, J. S., Stanek, K. Z., et al. 2017a, MNRAS, 467, 1098
Holoien, T. W.-S., Brown, J. S., Stanek, K. Z., et al. 2017b, MNRAS, 471, 4966
Holoien, T. W.-S., Prieto, J. L., Kochanek, C. S., et al. 2014, ATel, 6436, 1
Holoien, T. W.-S., Stanek, K. Z., Kochanek, C. S., et al. 2017c, MNRAS, 464, 2672
Howell, D. A., & Murray, D. 2010, CBET, 3313, 2
Howerton, S., Drake, A. J., Djorgovski, S. G., et al. 2011, CBET, 2658, 1
Huang, F., Wang, X., Zampieri, L., et al. 2016, ApJ, 832, 139
Huang, F., Wang, X., Zhang, J., et al. 2015, ApJ, 807, 59
Indebetouw, R., Matsuura, M., Dwek, E., et al. 2014, ApJL, 782, L2
Inserra, C., Fraser, M., Smartt, S. J., et al. 2016, MNRAS, 459, 2721
Itagaki, K., Brimacombe, J., Noguchi, T., & Nakano, S. 2011, CBET, 2943, 1
Jencson, J. E., Kasliwal, M. M., Adams, S. M., et al. 2018, ApJ, 863, 20
Jencson, J. E., Kasliwal, M. M., Johansson, J., et al. 2017, ApJ, 837, 167
Jha, S., Branch, D., Chornock, R., et al. 2006, AJ, 132, 189
Jin, Z., Gao, X., McCully, C., & Jha, S. W. 2013, CBET, 3520, 1
Johansson, J., Goobar, A., Kasliwal, M. M., et al. 2017, MNRAS, 466, 3442
Kamble, A., Margutti, R., Soderberg, A. M., et al. 2016, ApJ, 818, 111
Kankare, E., Fraser, M., Ryder, S., et al. 2014, A&A, 572, 75
Kasliwal, M. M. 2010, ATel, 2379, 1
Kasliwal, M. M., Bally, J., Masci, F., et al. 2017, ApJ, 839, 88
Kasliwal, M. M., Howell, J. L., Fox, D., Quimby, R., & Gal-Yam, A. 2009, ATel, 2218, 1
Kochanek, C. S., Szczygiel, D. M., & Stanek, K. Z. 2011, ApJ, 737, 76
Kotak, R., Meikle, W. P. S., Farrah, D., et al. 2009, ApJ, 704, 306
Kotak, R., Meikle, W. P. S., Pozzo, M., et al. 2006, ApJL, 651, L117
Kotak, R., Meikle, W. P. S., van Dyk, S. D., Höflich, P. A., & Mattila, S. 2005, ApJL, 628, L123
Kozasa, T., Nozawa, T., Tominaga, N., et al. 2009, in ASP Conf. Ser. 414, Cosmic Dust—Near and Far, ed. T. Henning, E. Grün, & J. Steinacker (San Francisco, CA: ASP), 43
Kumar, B., Pandey, S. B., Eswaraiah, C., & Kawabata, K. S. 2016, MNRAS, 456, 3157
Lennarz, D., Altmann, D., & Wiebusch, C. 2012, A&A, 538, A120
Leonard, D. C., Pignata, G., Dessart, L., et al. 2013, ATel, 5275, 1
Li, W., Cenko, S. B., & Filippenko, A. V. 2009a, CBET, 1656, 1
Li, W., Cenko, S. B., & Filippenko, A. V. 2009b, CBET, 1952, 1
Li, W., Foley, R. J., & Filippenko, A. V. 2004, IAUC, 8345, 4
Maeda, K., Hattori, T., Milisavljevic, D., et al. 2015a, ApJ, 807, 35
Maeda, K., Nozawa, T., Nagao, T., & Motohara, K. 2015b, MNRAS, 452, 3281
Margutti, R., Kamble, A., Milisavljevic, D., et al. 2017, ApJ, 835, 140
Margutti, R., Milisavljevic, D., Soderberg, A. M., et al. 2014, ApJ, 780, 21
Marion, G. H., Foley, R. J., & Calkins, M. 2012, CBET, 3106, 2
Marples, P., & Drescher, C. 2009, CBET, 2080, 1
Marples, P., Drescher, C., Quirk, S., & Bock, G. 2009, CBET, 1856, 1
Matheson, T., Jha, S., Challis, P., Kirshner, R., & Calkins, M. 2001, IAUC, 7761, 2
Matsuura, M., Dwek, E., Barlow, M. J., et al. 2015, ApJ, 800, 50
Matsuura, M., Dwek, E., Meixner, M., et al. 2011, Sci, 333, 1258
Mattila, S., Meikle, W. P. S., Lundqvist, P., et al. 2008, MNRAS, 389, 141
Mauerhan, J. C., Smith, N., Filippenko, A. V., et al. 2013, MNRAS, 430, 1801
Mauerhan, J. C., Van Dyk, S. D., Johansson, J., et al. 2017, ApJ, 834, 118
Maza, J., Hamuy, M., Antezana, R., et al. 2009, CBET, 1937, 1
Maza, J., Hamuy, M., Antezana, R., et al. 2010a, CBET, 2125, 1
Maza, J., Hamuy, M., Antezana, R., et al. 2010b, CBET, 2388, 1
McClelland, C. M., Garnavich, P. M., Milne, P. A., et al. 2013, ApJ, 767, 119
Meikle, W. P., Farrah, D., Fesen, R., et al. 2005, sptz prop, 20256
Meikle, W. P. S., Kotak, R., Farrah, D., et al. 2011, ApJ, 732, 109
Meikle, W. P. S., Mattila, S., Gerardy, C. L., et al. 2006, ApJ, 649, 332
Meikle, W. P. S., Mattila, S., Pastorello, A., et al. 2007, ApJ, 665, 608
Meng, X., & Podsiadlowski, Ph. 2018, ApJ, 861, 127
Milisavljevic, D., Margutti, R., Kamble, A., et al. 2015, ApJ, 815, 120
Modjaz, M., Kirshner, R., Challis, P., et al. 2005, IAUC, 8461, 2
Monard, L. A. G. 2009, CBET, 1798, 1
Monard, L. A. G., & Li, W. 2002, IAUC, 7940, 1
Monard, L. A. G., & Prieto, J. L. 2011, CBET, 2759, 1
Monard, L. A. G., Prieto, J. L., & Seth, K. 2011a, CBET, 2799, 1
Monard, L. A. G., Valenti, S., & Benetti, S. 2011b, CBET, 2749, 1
Moore, M., Li, W., Filippenko, A. V., Chornock, R., & Foley, R. J. 2004, IAUC, 8286, 2
Morrell, N., Folatelli, G., Hamuy, M., & Phillips, M. M. 2006, CBET, 368, 1
Morrell, N., & Phillips, M. M. 2009, CBET, 1953, 1
Müller, T., Prieto, J. L., Pejcha, O., & Clocchiatti, A. 2017, ApJ, 841, 127
Nagao, T., Maeda, K., & Yamanaka, M. 2017, ApJ, 835, 143
Nakano, S., Hirose, Y., & Li, W. 2005, IAUC, 8475, 1
Nakano, S., Kadota, K., Ikari, Y., & Itagaki, K. 2009, CBET, 1718, 1
Nakano, S., Kadota, K., & Itagaki, K. 2010, CBET, 2115, 1
Nakano, S., Kushida, R., & Kushida, Y. 2004a, IAUC, 8344, 1
Nakano, S., Kushida, R., Kushida, Y., & Itagaki, K. 2004b, IAUC, 8272, 1
Nakano, S., Yusa, T., Yoshimoto, K., et al. 2012, CBET, 3263, 1
Navasardyan, H., & Benetti, S. 2009, CBET, 1806, 1
Navasardyan, H., Benetti, S., Bufano, F., & Pastorello, A. 2009, CBET, 1738, 1
Nozawa, T., Kozasa, T., Umeda, H., Maeda, K., & Nomoto, K. 2003, ApJ, 598, 785
Nozawa, T., Maeda, K., Kozasa, T., et al. 2011, ApJ, 736, 45
Ochner, P., Siviero, A., Tomasella, L., et al. 2014, ATel, 5767, 1
Ofek, E. O., Sullivan, M., Cenko, S. B., et al. 2013, Natur, 494, 65
Papenkova, M., Li, W. D., Wray, J., Chleborad, C. W., & Schwartz, M. 2001, IAUC, 7722, 1
Pastorello, A., Cappellaro, E., Inserra, C., et al. 2013, ApJ, 767, 1
Patat, F., Cappellaro, E., Danziger, J., et al. 2001, ApJ, 555, 900
Pejcha, O., & Prieto, J. L. 2015, ApJ, 806, 225
Phillips, M. M., Simon, J. D., Morrell, N., et al. 2013, ApJ, 779, 38
Pignata, G., Cifuentes, M., Maza, J., et al. 2011, CBET, 2623, 1
Ponticello, N. J., Khandrika, H., Madison, D. R., et al. 2006, IAUC, 8709, 1
Pooley, D., & Lewin, W. H. G. 2004, IAUC, 8323, 2
Pozzo, M., Meikle, W. P. S., Fassia, A., et al. 2004, MNRAS, 352, 457
Prieto, J. L. 2011a, CBET, 2759, 2
Prieto, J. L. 2011b, ATel, 3615, 1
Prieto, J. L., Lee, J. C., Drake, A. J., et al. 2012, ApJ, 745, 70
Prieto, J. L., McMillan, R., Bakos, G., & Grennan, D. 2011, CBET, 2903, 1
Prieto, J. L., & Seth, K. 2011, CBET, 2799, 2

Puckett, T., Reddy, V., & Li, W. 2006, CBET, 363, 1
Quinn, J., Baade, D., Clocchiatti, A., et al. 2008, CBET, 1510, 1
Reach, W. T., Rho, J., Tappe, A., et al. 2006, AJ, 131, 1479
Sahu, D. K., Arora, S., & Anto, P. 2011a, CBET, 2658, 2
Sahu, D. K., Gurugubelli, U. K., Anupama, G. C., & Nomoto, K. 2011b, MNRAS, 413, 2583
Salvo, M., & Price, P. 2002, IAUC, 7947, 2
Shappee, B. J., Prieto, J. L., Grupe, D., et al. 2014, ApJ, 788, 48
Shurpakov, S., Balanutsa, P., Lipunov, V., et al. 2012, ATel, 4104, 1
Silverman, J. M., Kandrashoff, M. T., & Filippenko, A. V. 2009, CBET, 1968, 1
Silverman, J. M., Nugent, P. E., Gal-Yam, A., et al. 2013, ApJS, 207, 3
Siviero, A., Tomasella, L., Pastorello, A., et al. 2012, CBET, 3054, 4
Skrutskie, M. F., Cutri, R. M., Stiening, R., et al. 2006, AJ, 131, 1163
Smith, N., Silverman, J. M., Chornock, R., et al. 2009, ApJ, 695, 1334
Soderberg, A. M., Gal-Yam, A., & Kulkarni, S. R. 2004, GCN, 2586, 1
Stockdale, C. J., Weiler, K. W., van Dyk, S. D., et al. 2004, IAUC, 8282, 2
Stritzinger, M., Prieto, J. L., Morrell, N., & Pignata, G. 2011, CBET, 2623, 2
Stritzinger, M., Taddia, F., Fransson, C., et al. 2012, ApJ, 756, 173
Sugerman, B. E. K. 2003, AJ, 126, 1939
Sugerman, B. E. K., Ercolano, B., Barlow, M. J., et al. 2006, Sci, 313, 196
Szalai, T., & Vinkó, J. 2013, A&A, 549, A79
Szalai, T., Vinkó, J., Balog, Z., et al. 2011, A&A, 527, A61
Szalai, T., Vinkó, J., Nagy, A. P., et al. 2016, MNRAS, 460, 1500
Szczygiel, D. M., Kochanek, C. S., & Dai, X. 2012, ApJ, 760, 20
Taubenberger, S., Pastorello, A., Mazzali, P. A., et al. 2006, MNRAS, 371, 1459
Thrasher, P., Li, W., & Filippenko, A. V. 2008, CBET, 1507, 1
Tinyanont, S., Kasliwal, M. M., Fox, O. D., et al. 2016, ApJ, 833, 231
Tomasella, L., Pastorello, A., Valenti, S., & Benetti, S. 2011, CBET, 2934, 2
Valenti, S., Pastorello, A., Cappellaro, E., et al. 2012, ATel, 4076, 1
Van Dyk, S. 2013, AJ, 145, 118
Vinkó, J., Pooley, D., Silverman, J. M., et al. 2017, ApJ, 837, 62
Wesson, R., Barlow, M. J., Matsuura, M., & Ercolano, B. 2015, MNRAS, 446, 2089
Williams, B. J., & Fox, O. D. 2015, ApJL, 808, L22
Xue, M., Jiang, B. W., Gao, J., et al. 2016, ApJS, 224, 23
Yamanaka, M., Maeda, K., Tanaka, M., et al. 2016, PASJ, 68, 68
Zheng, W., Li, W., Filippenko, A. V., & Cenko, S. B. 2014, ATel, 5770, 1